To the Graduate Council:
I am submitting herewith a thesis written by Naiyu Wang entitled "Modeling and Analysis of the DuPont Access Bridge". I have examined the final electronic copy of this thesis for form and content and recommend that it be accepted in partial fulfillment of the requirements for the degree of Master of Science, with a major in Civil Engineering.

Edwin G. Burdette

Major Professor

We have read this thesis and recommend its acceptance:

David W. Goodpasture

J. Harold Deatherage

Acceptance for the Council:

Anne Mayhew

Vice Chancellor and Dean of Graduate Studies

(Original signatures on file with official student records)

MODELING AND ANALYSIS OF THE DUPONT ACCESS BRIDGE

A Thesis
Presented for the
Master of Science
Degree
The University of Tennessee, Knoxville

Naiyu Wang
August 2005

Dedication

This work is dedicated to my parents Dingyi Wang and XueFang Zhang for their tireless encouragement and inspiration. This work is also dedicated to my major professor and advisor, Dr. Edwin G. Burdette, whose support and guidance made this work possible.

Acknowledgements

I would like to thank all those that assisted me in earning the Master of Science Degree at The University of Tennessee. I would like to thank Dr. David Goodpasture and Dr. Harold Deatherage for serving on my committee and sharing their rich experiences with me. I would like to thank Dr. Earl Ingram, David Chapman and Dr. Ramzi Abdul-Ahad for their contributions to this project. I would like to thank Alan Tackie for his generous help during my study at UT.

Abstract

This thesis evaluates the lateral wheel load distribution on a two-span experimental highway bridge, examines the continuity of the superstructure over the center pier, and investigates the connection between bridge girders and abutments. Simplified finite element models of the bridge superstructure with different boundary conditions were made during the research to simulate the bridge behavior and verify the field data. Live load distribution factors for moment from the model with a rotational spring connection between bridge girders and abutment correlated well with factors from field measurements, and they were compared with factors from other methods currently in use such as AASHTO 1996, Henry's Method, and AASHTO LRFD Specifications. Moment transferred from strain measurements close to the center pier also compared favorably with the output from the single girder computer model with continuous boundary condition over the center pier and a rotational spring boundary condition at the ends. Therefore, the splice connection over the center pier appears to have created full continuity between the two spans.

Table of Contents

List of Tables

List of Figures

List of Figures

Figure Page

Chapter 1

INTRODUCTION

1.1 The DuPont Bridge

A research contract between the Tennessee Department of Transportation (TDOT) and The University of Tennessee was executed with a beginning date of September 1, 2003. The research involved the instrumentation, testing, and analysis of data for an experimental bridge over U.S. Highway 70 providing access to the DuPont plant in Humphreys County west of Waverly, Tennessee. Figures 1[*] and 2 show the plan and a photograph of the DuPont Bridge.

The DuPont Bridge is a two-span access bridge supported by integral abutments at each end and a pier between the east and west bound lanes. The superstructure of the bridge consists of a concrete deck and six steel girders. The girders are W33x240 spaced at 7'-4" (2.24 m) on center. To resist lateral torsional buckling, C15x33.9 channels are bolted to the plate stiffeners on the girders. Connection of the girders over the pier was achieved by 1⅝" (4.13 cm) thick, 11'-3½" (3.44 m) long cover plates on the top flanges. The compression forces at the pier are transferred between girders by a 1⅞" (4.76 cm) thick wedge kicker plate that is two

[*] All tables and figures are located in the appendix.

inches wider than the bottom cover plate and bears against the inside of the bottom flange. The concrete decking is 8¼" (20.9 cm) thick, and acts compositely with the girders.

1.2 Scope

This bridge was designed to act continuously over the center pier under the dead load of the concrete deck. Field Testing was conducted by personnel in the Civil Engineering Department of the University of Tennessee to evaluate the effectiveness of the design in providing the desired continuity over the center pier and to measure load distribution under the action of a loaded vehicle.

In this thesis, simplified finite element models were made to simulate the bridge behavior. Output from the models were compared with the field measurement (a) to investigate continuity over the middle pier, (b) to evaluate live load distribution for moment under the action of a loaded vehicle and (c) to analyze the connection between bridge girders and the integral abutments.

Chapter 2

LITERATURE REVIEW

2.1. Lateral Load Distribution

In 1997, a typical one-span, two-lane, simply supported, composite steel girder bridge was selected to compare the performance of four finite element modeling techniques employed by various researchers and to evaluate the effectiveness of different formulas for calculating wheel load distribution factors (Mabsout et al. 1997). Under the same discretization and load position, the four finite element modeling techniques yielded similar load distribution factors. Their choices of finite element programs were SAP90 and ICES-STRUDL. Further parametric study, which varied the span length and girder spacing, was conducted and the results from two of the four finite modeling techniques correlated well with AASHTO LRFD specifications. In one model, the concrete slab was idealized as quadrilateral shell elements and the steel girder as a space frame member, and in the other model, the concrete slab was idealized using isotropic eight node brick elements, and steel girder flanges and webs were modeled using quadrilateral shell elements. The paper concluded that the AASHTO LRFD equation can be applied with confidence in the analysis and design of single and multispan, composite and noncomposite, straight steel bridges. The AASHTO (1996) distribution factor was shown to be conservative when compared with experimental results and with finite element modeling techniques.

The finite element modeling of the Roebling suspension bridge over the Ohio River between Covington, Kentucky and Cincinnati, Ohio by Ren, Harik, Lenett, and Baseheart had aspects similar to the work presented herein. From the structural evaluation scheme of the Roebling suspension bridge, they were able to create a 3D finite element model using the ANSYS finite element modeling software. The result of their Finite Element Method (FEM) analysis was compared with in-situ ambient vibration measurements, and good agreement was found. Their calibrated model served as a baseline for the structural evaluation of the bridge. The outcome assisted in the preservation of the Roebling suspension bridge, and their methodology was applied in later cases to a wide range of cable-stayed bridges.

The I-40 Bridge over the Rio Grande in Albuquerque, New Mexico, was studied by Farrar and Duffey in 1998. Their work addressed simplified modeling of composite bridges subjected to dynamic loading with particular emphasis on torsional response. They used a single beam element to represent the cross section of the composite girder-slab bridge undergoing bending and torsional deformation. The challenges they faced in using simplified elements in their FEM were comparable to those encountered during the modeling of the bridge analyzed in this paper.

2.2. Continuity Over Center Pier

Most bridges are designed to act continuously over the piers. The DuPont Bridge as previously mentioned is not common in the sense that the two spans supported over the middle pier were erected as simply supported spans with connection plates at the top and bottom flanges to simulate a continuous bridge. There are therefore not many precedents to which one can look to for comparison. The approach taken during the DuPont investigation of continuity was to compare results from a simulating computer model to the field measurements.

Chapter 3

MODELING IN THIS THESIS

Modeling in this thesis was accomplished using Visual Analysis which is a finite element software package that is relatively simple to use. It permits users to choose from a variety of steel shapes incorporated in a database and to define different support conditions and material properties.

Two sets of computer models, single girder models and whole superstructure models, were created using Visual Analysis to analyze the bridge behavior and compare the output with experimental data. The first set of single girder models was made to investigate the effectiveness of design continuity over the middle pier under the deck load. Each model consisted of the north and south spans of a girder with different boundary conditions at the ends and over the center pier. In each model, the unique connection of the DuPont Bridge over the center pier was considered. A detailed discussion of this connection and the single girder models is presented in Chapter 4.

The second set modeled the whole superstructure of the bridge with different boundary conditions for the purpose of evaluating the lateral live load distribution on girders. Each model consisted of two spans of six girders, concrete deck, and abutments. The modeling phases and details of analyses are presented in Chapter 5.

Chapter 4

CONTINUITY

This Chapter was originally written primarily by Dr. Earl Ingram. My contribution to work introduced in this chapter was computer modeling and providing model output.

4.1 Introduction

Strain gage data collected during the placement of the concrete deck were analyzed in an effort to verify the level of continuity created by the girder connection at the center pier. The connection detail at the center pier allowed for the two spans to be erected as two simply-supported spans and then joined with a bolted splice-plate connecting the top flanges and a welded wedge plate connecting the bottom flanges. The magnitude of moment generated by loads encountered during the concrete deck pour was measured at various locations along the length of the girders and compared to computer analyses that assumed various boundary conditions. Conclusions were drawn regarding the existing level of continuity by matching measured behavioral characteristics to results predicted by the computer models.

4.2 Data Collection

Gages were placed on the three girders on the south span that are west of the bridge centerline. The exterior girder was designated as

Girder E, while the first interior girder was labeled Girder F, and the second interior girder was named Girder G. Gage locations are illustrated in Figure 3. All three girders received strain gages adjacent to the face of the concrete diaphragm at the center pier (Location P), 3 ft from the face of the concrete diaphragm at the center pier (Location P3), and 34 ft from the face of the integral abutment (Location IA34). In addition, Girder F received gages located 6 inches from the face of the integral abutment (Location IA). Locations P3 and IA34 each received four gages on each girder: one gage on the inside face of the bottom flange, one gage located at one-third of the girder depth on the web, one gage located at two-thirds of the girder depth on the web, and one gage on the inside face of the top flange. Space restrictions due to forming materials resulted in the placement of only a single gage located on the inside face of the bottom flange at Location P. Gage number 2 was at Location P, gages 3 thru 6 were at Location P3, gages 7 thru 10 were at Location IA34, and 11 thru 14 were at Location IA (on Girder F only).

All gages were "zeroed" immediately before placement of the concrete bridge deck, which was after completion of the form construction and rebar placement. Therefore, the only load measured by the gages was the load caused by the concrete itself. Data were collected at a sampling rate of two samples per second. Sampling began at the start of the placement operation and continued, uninterrupted, until approximately five minutes after completion of the deck pour.

4.3 Measured Results

The results that were used to verify continuity were those collected during the last five minutes of the test, which was after all of the concrete had been placed. The means of the 600 data readings that were collected for each gage during the last five minutes were used as the official strain readings for analyses. At each location that contained multiple strain readings through the depth of the girder, a plot was generated relating measured strain to the vertical location of the gage relative to the bottom flange of the girder. In theory, these plots should show a linear relationship between strain and vertical location through the cross-section. By analyzing the strain versus depth plots, erroneous strain readings were identified and eliminated from subsequent analyses. However, very few data points were eliminated based on these plots with the exception of data collected at Location IA on Girder F. A thorough analysis of all data collected at Location IA from the beginning of the concrete pour indicated that only Gage F14 was functioning properly. Therefore, results for Location IA are based on readings from a single gage.

After generating the strain versus depth plots and deleting invalid points, a linear regression line was created for strain versus depth at each cross-section investigated. The strain versus depth plots are shown in Figures 4 thru 9 where compressive strain is plotted at the right side of each figures. A range of valid strain readings for the top and bottom flanges at each location was defined as the range of values between the measured data points and the regression line. The strain ranges were then converted into moment ranges that could be compared to results obtained from a computer analysis. A summary of the ranges of measured moment at Locations P3 and IA34 is presented in Table1.

Converting strain readings to moment magnitude requires knowledge regarding the placement of the gage, modulus of elasticity of the material, and moment of inertia of the cross-section. In the case of Locations P and P3, determining the effective moment of inertia required an analysis of the development length of the 1-5/8 inch thick bolted splice-plate on the top flange and the welded ½ inch cover plate on the bottom flange. Both plates were assumed fully developed at Location P. Based on calculations considering the bolt and weld details, it was determined that the 1-5/8 inch thick plate was approximately 50% developed at Location P3, while the ½ inch thick cover plate was fully developed. The location of the neutral axis and magnitude of the effective moment of inertia were then calculated for Location P3 assuming top and bottom cover plate thicknesses of 13/16 and ½ inch, respectively. The calculated location of the neutral axis was then compared to the y-intercept of the regression lines for strain gage readings collected at Location P3. Agreement between the calculated and measured neutral axis indicates that the assumptions regarding cover plate development are plausible.

4.4 Computer Models

Computer models were created using Visual Analysis to predict moment along the length of the girders during the placement of the concrete deck. Each girder was modeled individually. Each model consisted of the north and south spans, supports at both abutments, and the support at the center pier. Each span was divided into two parts. The part close to the abutment had a cross-section of steel girder W33 x 241, the other close to the center pier had a composite cross–section of girder plus top and bottom cover plates. Three different boundary conditions BC1, BC2 & BC3 were investigated. The first set of boundary conditions (BC1) represented simply supported spans. The second set of boundary conditions (BC2) assumed that the girders were continuous over the center pier and simply supported at the integral abutments. The final set of boundary conditions (BC3) assumed that the girders were continuous over the center pier and rotationally resisted at the integral abutments by springs with a stiffness of 1000 K-ft/deg. The third model was created in an effort to accurately represent rotational resistance produced by embedding the girders into the integral abutments.

The bridge plans specify a deck thickness of 8-1/4 inches, with the concrete slab poured on metal decking that spans between girders in a simply supported fashion. A uniformly distributed load was calculated based on girder spacing, slab thickness, and concrete unit weight. The load was applied to the entire length of the girder models and compared to the measured results. Girders F and G were subjected to identical field loading, thereby justifying one set of computer models to represent both girders. Girder E was subjected to a slightly lower field loading due to the short overhang of the deck extending towards the exterior of the bridge. Therefore, a separate set of models with different loading was used when analyzing the behavior of Girder E. Figure 10 shows the three moment diagrams for the both span created from the computer models for Girder E along with measured data points. Figure 11 shows the same information for Girders F and G.

4.5 Discussion of Results

Figures 10 and 11 show that measured results were most accurately predicted by the model with BC3, which is the model that incorporated continuity at the center pier and a rotational spring at each integral abutment. A comparison of measured results to those obtained from model BC3 shows that the model is appropriately shaped to the measured data, especially at location IA34 where the moments converted from strain measurements are most reliable due to the absence of any added moment of inertia to the rolled shape, but the model slightly over-predicted the moment magnitude at Locations P3. This fact led to the conclusion that the uniformly distributed load used in the computer model might be slightly overestimated. Because only one gage was placed at Location P on each girder, it was impossible to verify the assumption regarding splice-plate development using a neutral axis comparison. However, had the top splice-plate been fully developed, the effective moment of inertia would have Increased, consequently increasing the calculated moment from strain data.

Boundary condition set BC2 also over-predicted the moment magnitudes at Locations P3, and it also over-predicted the moment magnitudes at location IA34. The measured data at Location IA34 was the most reliable of all of the locations due to the absence of any added moment of inertia to the rolled shape and the measurement of a complete strain profile through the depth of the section. Therefore, the over-prediction of moment at Location IA34, coupled with the larger over-prediction of the moment at location P3, indicated that BC2 was not an accurate representation of the behavior of the girders.

Boundary condition set BC1 did not appear to accurately represent measured data anywhere along the length of the girders. Therefore, the assumption that the bridge may behave as two simply-supported spans was dismissed.

4.6 Conclusion

The continuity created by the splice-connection at the center pier is evident by the measurement of negative moment 3 feet from the center pier. Furthermore, the magnitude of positive moment measured near the mid-span closely agrees with that expected when assuming continuous behavior of the bridge over the center pier. In the event that the connection was providing limited continuity, model BC3 would have over estimated negative moment near the center pier and under estimated positive moment at Location IA34. However, this phenomenon did not occur. The measured positive moment at Location IA34 was accurately predicted by moment output from a model assuming full continuity. Therefore, the splice connection over the center pier appears to have created the desired full continuity between the two spans over the center pier of the DuPont bridge.

Chapter 5

LATERAL DISTRIBUTION OF LOAD

5.1 Introduction

Wheel load distribution in highway bridges is very important in designing new bridges and evaluating existing ones. The load distribution is affected by the location of the truck, the magnitude of the truck load, and the type of bridge superstructure. There are different formulas for evaluating load distribution. AASHTO, the governing authority on road and bridge design and analysis, has specifications for a single lane of wheel loads for a design truck or lane loading. The load distribution factor S/5.5, (S is girder spacing in feet), was used for many years to calculate the moment in an individual girder. Recent AASHTO specifications introduced new load distribution formulas which depend on the span, spacing, and geometric cross-section of the bridge. In this chapter, simplified finite element models of the DuPont superstructure with different boundary conditions were made to simulate the bridge behavior. The output of these models was compared with the load distribution factors obtained from field measurements and with factors from other methods currently in use such as AASHTO 1996, Henry's Method, and AASHTO LRFD Specifications.

5.2 Current Methods for Lateral Load Distribution

The following methods are, or have been, used to determine lateral load distribution on highway bridges. The finite element results obtained later herein were compared to the results from these methods as well as to the results obtained from field measurements.

AASHTO 1996

The distribution of moments on interior and exterior stringers is the product of wheel load moment and the factor S/5.5, where S is the spacing between girders in feet.

DuPont Bridge – AASHTO 1996:

The factor for wheel load moment in one girder = S/5.5 = 7.33/5.5/2 = 0.666.

HENRY'S METHOD

This method, which was created in 1963 for calculating lateral distribution of live load moment in longitudinal girders, assumes equal distribution to all girders and was developed by former TDOT Engineer of Structures, Henry Derthick. The calculations of live load moment distribution factors for prestressed I–beams and steel beams are shown below.

(a) Based on a 10 ft. (3.05 m) traffic lane width, the fractional number of design traffic lanes is obtained by dividing the roadway width by 10.

(b) The Live Load Reduction Factor (LLRF) expressed as a percentage is obtained by linearly interpolating the number of traffic lanes obtained in step (a) from the scale given below.

2 lanes = 100%
3 lanes = 90%
4 lanes = 75%

(c) Multiply the LLRF in (b) by the number of traffic lanes obtained in (a) and divide the product by the number of beams.

(d) Multiply (c) by 2 for number of rows of wheels per beam.

(e) Multiply (d) by the ratio 6/5.5 to get the Live Load Moment Distribution Factor for girders.

DuPont Bridge – Henry's method:

Roadway width = 40 ft. (3.05 m)

Number of Girders = 6

- 40/10=4
- LLRF= 0.75 (4 lanes)
- 0.75*4/6=0.5
- 0.5*2=1.0
- 1.0*6/5.5=1.09
- 1.09/2=<u>0.545</u> (Moment distribution factor on one girder for truck load)

AASHTO LRFD

For concrete deck on steel beams, the live load distribution for moment in girders can be calculated using the following equations:

Interior Girders:

One Design Lane Loaded:

$$g_{int} = 0.06 + (\frac{S}{14})^{0.4}(\frac{S}{L})^{0.3}(\frac{K_g}{12.0 \cdot Lt_s^3})^{0.1}$$

Two or More Design Lanes Loaded:

$$g_{int} = 0.075 + (\frac{S}{14})^{0.6}(\frac{S}{L})^{0.2}(\frac{K_g}{12.0 \cdot Lt_s^3})^{0.1}$$

Where:

g_{int} = distribution factor for interior beams

S = Spacing of beams or webs (ft)

L = Span length parameter (ft)

t_s = Depth of concrete slab (in)

Kg = Longitudinal stiffness parameter (in^4)

$$Kg = n(I + Ae_g^2)$$
$$n = \frac{E_B}{E_D}$$

E_B = Modulus of elasticity of beam material (ksi)

E_D = Modulus of elasticity of deck material (ksi)

$I =$ Moment of inertia of beam (in^4)

$e_g =$ Distance between the centers of the basic beam and deck (in)

Exterior Girders:

One Design Lane Loaded:

For one design lane loaded, the live load distribution factor for exterior girders is computed using the lever rule. The lever rule is a method of computing the distribution factor by summing moments about the first interior girder to get the reaction at the exterior girder, assuming there is a rotational hinge in the bridge deck directly above the first interior girder.

Two or More Design Lanes Loaded:

$$g_{exterior} = e \cdot g_{interior}$$
$$e = 0.77 + \frac{d_e}{9.1}$$

Where: $g =$ Distribution factor

$e =$ Correction factor

$d_e =$ Distance from exterior web of exterior beam and the interior edge of curb or traffic barrier

DuPont Bridge – AASHTO LRFD:

For Positive Moment in Interior Girders:

$$g_{\text{int}} = 0.06 + \left(\frac{7.33}{14}\right)^{0.4}\left(\frac{7.33}{87}\right)^{0.3}\left(\frac{7.19 \times (14200 + 70.9 \times 21.2^2)}{12.0 \times 87 \times 8.25^3}\right)^{0.1} = \underline{0.407}$$

For Negative Moment in Interior Girders:

$$g_{\text{int}} = 0.06 + (\frac{7.33}{14})^{0.4}(\frac{7.33}{81.5})^{0.3}(\frac{7.19 \times (14200 + 70.9 \times 21.2^2}{12.0 \times 81.5 \times 8.25^3})^{0.1} = \underline{0.416}$$

For Moment in Exterior Girders:

The Lever Rule is used to calculate moment distribution in exterior girders. The two wheel lines of the design truck are 6 ft apart. One wheel line was placed on the exterior girder E, and the other was 6 ft from girder E and 1.33 ft from girder F as shown in Figure 12. From statics, $R_A = 0.591P$. The lane fraction carried by the exterior girder is $R_A/P = 0.591P/P = 0.591$. A multiple presence factor m=1.2 for a steel girder bridge should be used for the probability for multiple trucks passing over a multilane bridge simultaneously; therefore, the distribution factor for the exterior girder =1.2 x 0.591=0.709. In this research with one lane loaded, a factor of <u>0.591</u> was used for the exterior girders to compare with factors from field data and from computer models.

5.3 Field Testing & Data Collection

Field tests were conducted to determine the lateral load distribution in the girders. The controlled load test included 14 individual tests, each with the truck in a different position as shown in Table 2. The truck used in each test was a four axle Mack dump truck provided by TDOT. The truck was loaded with aggregate and weighed 73,500 lbs. with 19,470 lbs. on the front axle. In order to concentrate the loads, the movable axle was raised, making the truck illegal for normal road operations.

The first individual test, Test 1, was conducted to determine the locations on the bridge where the truck would be located to provide the maximum moments at the midspan and at the pier. These locations were identified by moving the truck slowly across the bridge from north to south and monitoring the strain readings at several gages. When a maximum reading occurred, the truck was stopped and the location was marked on the deck with chalk. Locations A and C shown in Figure 13 are the locations where the truck was located on the bridge to produce a minimum and maximum strain at the mid-span; location B is the point where the truck was to be located to produce a maximum strain at the pier.

After A, B and C were located, the remaining 13 individual tests were conducted to determine how the position of the load affects the moments on the bridge girders by moving the truck laterally on these locations as shown in Figure 14. Figure 15 shows the axial configuration of the control load truck. The truck front axial was located at points A, B, and C, respectively, for each test, with the truck headed left to right in figure 14. Test 2 data consisted of the strains collected when the truck ran in the southbound lane with the wheels on Girders E and F. Test 3 data consisted of the strains collected when the wheels of the truck were straddling girder F. In test 4, strains were collected when the truck were straddled girder G. Test 5 data consisted of the strains collected when the wheels of the truck were straddling the center line. Strain data collected during test 6 resulted from the truck straddling girder H. Test 7 data consisted of the strains collected with the truck wheels on Girders H and I. Test 8 data consisted of the strains collected when the truck straddled girder I. Test 9 data consisted of the strains readings when the truck wheels were on Girders I and J.

During Tests 2 through 9, the truck stopped at A, B, and C for 20 to 30 seconds to collect static data. Tests 10 and 11 were conducted with the truck on girder F & G and E & F respectively, moving at a low speed and without stopping at A, B, and C. Test 12, 13, and 14 were conducted with the truck running at a higher speed (25 to 30 mph) with wheels located on girder F and G. Table 2 summarizes how all the tests were conducted. The term static is taken to mean that the truck stopped at A, B, and C, also that it moved at 3 to 5 mph between points. The term rolling will be taken to mean that the truck moved at 25 to 30 mph and did not stop at A, B, or C.

Strain gages were installed at several cross sections along gliders E, F, & G. Each gage on a girder was identified by a number, and each number corresponded with a specific location on the girder. The location of Gage 7 as shown in Figure 16 on each of the cross sections of girder E, F, and G was 34 ft. (10.36 m) from the face of the south abutment and at the top flange of the sections. Gage E7 was the gage at position 7 on girder E. The vertical locations of the gages are shown in Figure 17.

The research trailer was located in a position where the deck was not easily visible. Two-way radios were used to coordinate the stopping and starting of the truck and the corresponding test on the Megadac. While some personnel in the trailer manipulated the Megadac, others directed the truck. During the test the same personnel that directed the truck also periodically opened and closed the bridge to traffic. TDOT provided assistance with traffic control efforts. The strain data were collected at 400 readings per second per gage.

5.4 Measured Results

Static strain data were taken when the truck was located laterally at longitudinal locations A, B, & C. Since moment is directly proportional to strain, the moment distribution of truck load to each girder was expressed as a percentage of the strain reading on individual girders to the sum of strain readings from all six girders. The gage chosen to determine load distribution was the gage on the bottom flange at each location of interest. The resulting percentages at each truck location were plotted in Figure 22 through Figure 36 along with the output from computer models. It was found that the longitudinal truck location had little effect on lateral load distributions. The exterior girder E experienced the maximum live load distributions of 0.415 and 0.548 for positive and negative moment respectively. The interior girders had maximum distributions of 0.378 for positive moment and 0.365 for negative moment. These values are tabulated in Table 3 and 4. A discussion and comparison of those value with the computed distributions using various methods and the output from computer models are presented later on in this chapter (Section 5.6).

5.5 Computer Models

The computer models were developed in phases. Improvements were made later on by refining the initial models. A discussion of the early models and subsequent improvements is presented here.

Girder

The DuPont access bridge has six girders, each identified by a letter; lettering began with "E" for Exterior. The girders were labeled from west to east. The superstructure of the bridge consists of the six steel girders, concrete deck and parapet, and they work together as a composite section. Figure 18 shows the cross-section of the composite section. Beam elements were used to represent the composite section. The effect of the parapet was considered during the calculation of the moment of inertia for girders. The exterior girders were more affected by the parapet than the interior girders. As a result of such effects, approximate equations for the moment of inertia for each of the girders were formulated and used in the distribution of load to each girder.

$$I_1 = I_2(1+\frac{1}{n}) = \frac{7}{6}I_2 = \frac{7}{36}I_c$$

$$I_2 = I_c(\frac{1}{n}) = \frac{1}{6}I_c = \frac{6}{36}I_c$$

$$I_3 = I_2(1-\frac{1}{n}) = \frac{5}{6}I_2 = \frac{5}{36}I_c$$

Where:

I_1: Moment of inertia for exterior girder E, J.

I_2: Moment of inertia for intermediate girder F, I.

I_3: Moment of inertia for interior girder G, H.

I_c: Moment of inertia for the whole bridge cross section

(girder + deck + parapets).

n: Number of girder, equal to 6.

Deck

Since the deck acts compositely with the girders, beam elements at 5 ft. (1.52 m) spacing between girders were created to simulate the stiffness of the concrete deck. In Figure 19, a mesh of the superstructure illustrates a VisualAnalysis representation of the model.

Connection between Bridge Girders and Abutments

Three different sets of boundary conditions between the bridge deck and the abutment were investigated. BC1 assumed continuity over the middle pier with simple supports at the abutments. BC2 assumed that the girders were continuous over the center pier and had fixed supports at the integral abutments, and the final boundary condition BC3 assumed that the girders were continuous over the center pier and resisted at the integral abutments with rotational springs with a stiffness of 5000 K-ft/deg. This value is larger than the 1000 K-ft/deg used in Chapter 4 because (a) the entire bridge is modeled here and (b) the slab has cured to form a composite section. The third boundary condition BC3 was created in an effort to accurately represent rotational resistance produced by embedding the girders into the integral abutments.

Improvements

Refinements of the models discussed above led to the use of plate elements to model the concrete deck instead of only using beam elements between girders to represent the stiffness of the slab. In addition, the parapet itself was modeled using beam elements in lieu of approximately distributing its influence on each girder according to the position between the parapet and girders. These changes enhanced the computer simulation by greatly improving the prediction of the behavior of exterior girders as shown in Figure 20 and Figure 21. It is apparent that the effect of parapets on exterior girders may have been over estimated in the early model. Results discussed later on in section 5.6 are based on the output from the improved model.

5.6. Discussion of Results

The lateral distribution of moments in the girders due to the truck loading at different locations is shown in Figure 22 through Figure 36. Each figure includes measured data and model output from three models distinguished by end boundary conditions. The figures indicated that output of computer models compared favorably with the field data, especially the one with a rotational spring boundary condition between girders and abutments. The figures also show that the lateral distribution factor for moment at each truck location was higher in those girders which were close to the truck load position and decreased for the far edge girders.

Live load distribution factors for positive moment and negative moment, from models, measurement, and different specifications, are tabulated in Table 3 and Table 4 respectively. It is shown that moment distribution factors for exterior girders are larger than the factors for interior girders.

It is also shown in Table 3 and Table 4 that the measurements had good agreements with AASHTO LRFD specifications on both positive moment distribution factors and negative moment distributions.

Henry's method is conservative for interior girders but very close to field measurements for the exterior girders. AASHTO 1996 is conservative for both interior and exterior girders.

5.7. Conclusion

- The finite element model with spring boundary condition correlated best with the experimental results.
- The distribution factors for moment from the computer model analysis and from field measurement both have good agreement with AASHTO LRFD on both interior girders and exterior girders.
- Henry's Method is a little conservative for interior girders, but compares favorably with measurements on exterior girders.
- AASHTO (1996) method is conservative for both interior and exterior girders.

Chapter 6

SUMMARY AND CONCLUSION

This thesis sought to verify the extent of continuity of the DuPont Bridge over the center pier and also to investigate the wheel load distribution for moment on girders.

A single girder computer model assuming full continuity over the center pier and rotational resistance between girders and abutment was made to analyze the continuity over the center pier. Negative moment calculated from strain measured 3 feet from the pier as well as positive moment from strain measured near the mid-span accurately matched the model output. It therefore can be concluded that the splice connection over the center pier appears to have created the desired full continuity between the two spans over the center pier of the DuPont bridge.

A model of the entire DuPont superstructure, assuming continuous behavior over the center pier and rotationally resisted at the integral abutments at a stiffness of 5000 k-ft/deg, yielded the best results in the verification of the measured load distribution. The factor calculated from AASHTO LRFD had good agreements with field measurement on both exterior girders and interior girders. Henry's method compared favorably with field data on the exterior girders but was a little conservative for the interior girders. AASHTO 1996 was conservative for both interior and exterior girders.

REFERENCES

REFERENCES

Burdette, E. G., Deatherage, J. H., Goodpasture, D. W. and Ingram, E. E. *(2004)*. "Evaluation of Experimental Bridge: DuPont Access Bridge in Humprhreys County, Final Report." University of Tennessee at Knoxville, Knoxville, Tennessee.

Farrar, C. R. and Duffey, T. A. *(1998)*. "Bridge Model Properties Using Simplified Finite Element Analysis." *Journal of Bridge Engineering, February 1998, 38-46.*

"LRFD Bridge Design Specifications." American Association of State Highway and Transportation Officials, Inc., *Third Edition, 2004*.

Mabsout, M. E., Tarhini, K. M., Frederick, G. R. and Tayar, C. *(1997)*. "Finite-Element Analysis of Steel Girder Highway Bridges." *Journal of Bridge Engineering, August 1997, 83-87*.

Ren, Wei-Xin, Harik, I.E., Lenett, M. and Baseheart, T. (2004). "Model Properties of the Roebling Suspension Bridge – FEM Modeling and Ambient Testing." *Journal of Bridge Engineering, ASCE, Vol.9, No.2*.

"VisualAnalysis User's Guide." By Integrated Engineering Software, Inc. *January 7, 2003*

"Live load Distribution Factors for a Three Span Continuous Precast Girder Bridge" By Staff - BridgeSight Software, *04/01/99,* www.bridgesite.com/bridgesightsol/FILES/lldf1.pdf.

APPENDIX

Tables and Figures

Table 1: Measured Moment Ranges at Locations P3 and IA34

	Location P3		Location IA34	
Girder	M_{min} (k-ft)	M_{max} (k-ft)	M_{min} (k-ft)	M_{max} (k-ft)
E	-343	-383	262	304
F	-311	-353	292	323
G	-378	-413	281	327

Table 2: Summary of Tests Performed

Test	Location of Truck							
	E	F	G	center line	H	I	J	Speed of Travel
1		X	X					static
2	X	X						static
3		X						static
4			X					static
5				X				static
6					X			static
7					X	X		static
8						X		static
9						X	X	static
10		X	X					static (without stopping)
11	X	X						static (without stopping)
12		X	X					rolling
13		X	X					rolling
14		X	X					rolling

Table 3: Distribution Factors for Positive Moment

Girder	AASHTO (1996)	HENRY METHOD	AASHTO LRFD	COMPUTER ANALYSIS			FIELD MEASUREMENTS
				Pinned	Fixed	Spring	
E(Exterior Girder)	0.666	0.545	**0.591**	0.400	0.443	**0.418**	**0.415**
F(Interior Girder)			**0.407**	0.335	0.414	**0.357**	**0.378**
G(Interior Girder)				0.300	0.386	0.322	0.329

Table 4: Distribution Factors for Negative Moment

Girder	AASHTO (1996)	HENRY METHOD	AASHTO LRFD	COMPUTER ANALYSIS			FIELD MEASUREMENTS
				Pinned	Fixed	Spring	
E(Exterior Girder)	0.666	0.545	**0.591**	0.458	0.472	**0.464**	**0.548**
F(Interior Girder)			**0.416**	0.345	0.378	**0.357**	0.289
G(Interior Girder)				0.342	0.376	0.351	**0.365**

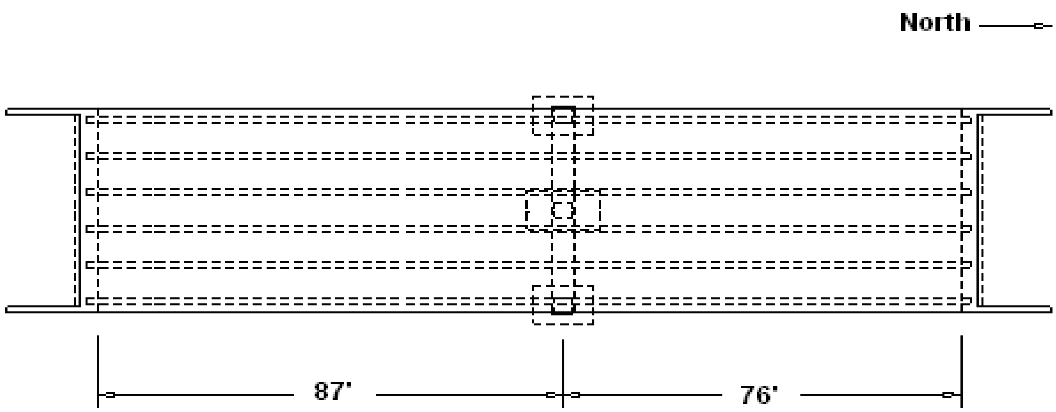

Figure 1: Plan View of the DuPont Bridge

Figure 2: Photo of the DuPont Bridge

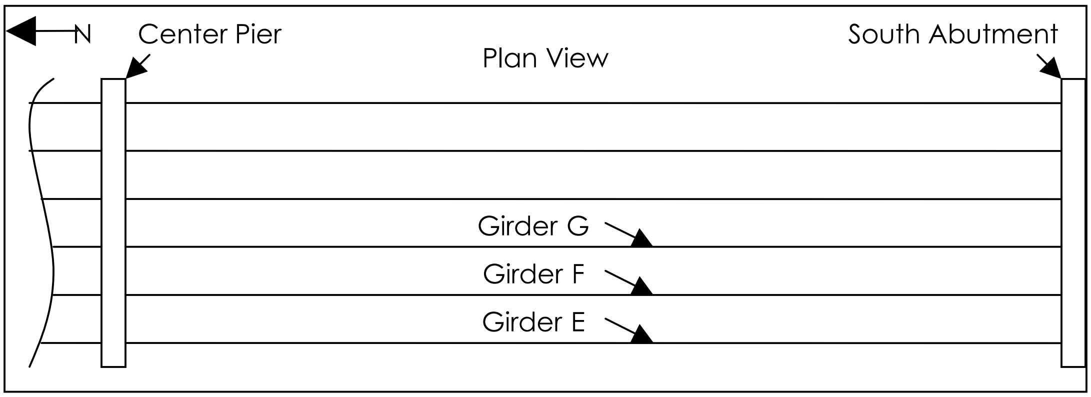

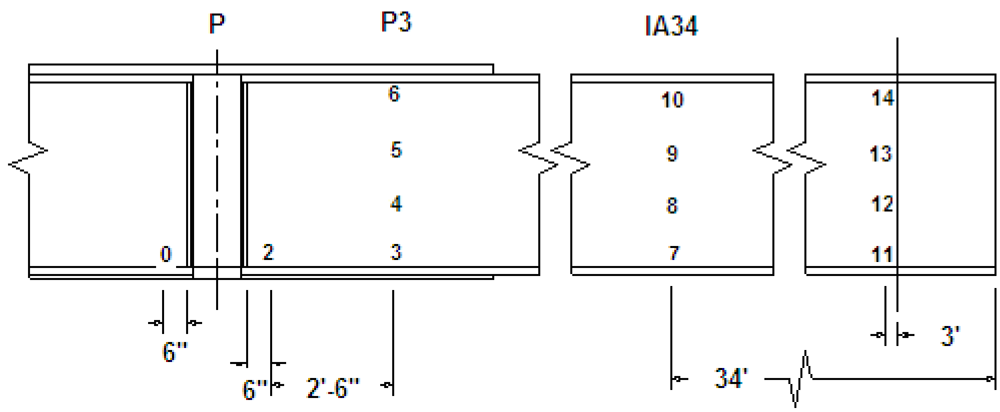

Figure 3: Girder Labeling and Gage Numbering

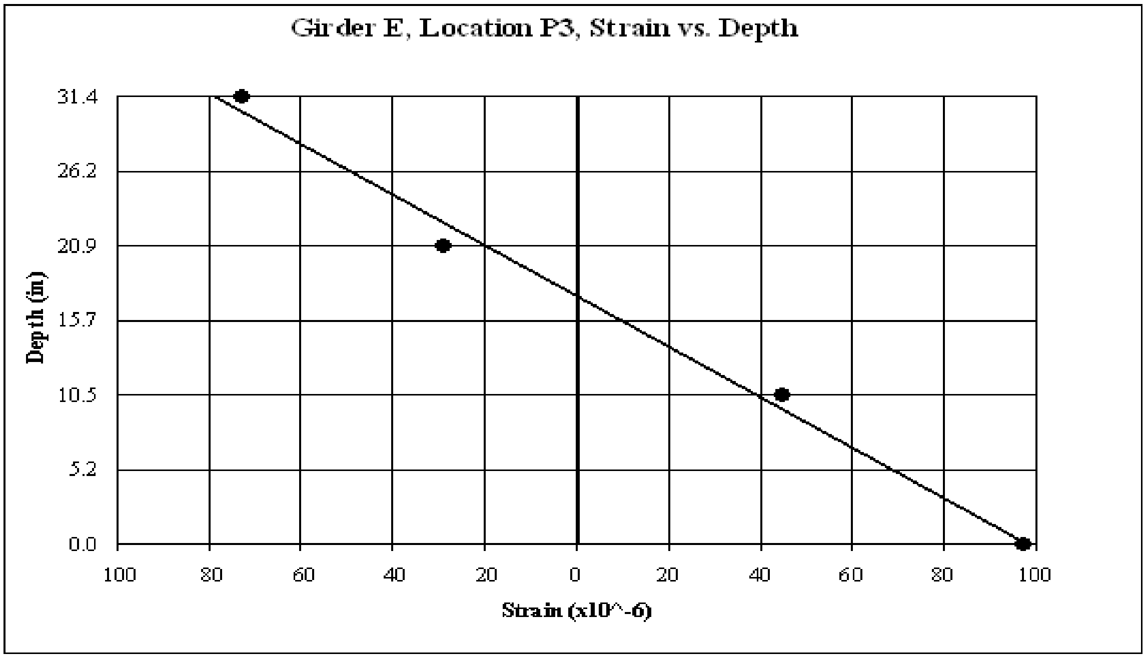

Figure 4: Girder E, Location P3, Strain vs. Depth

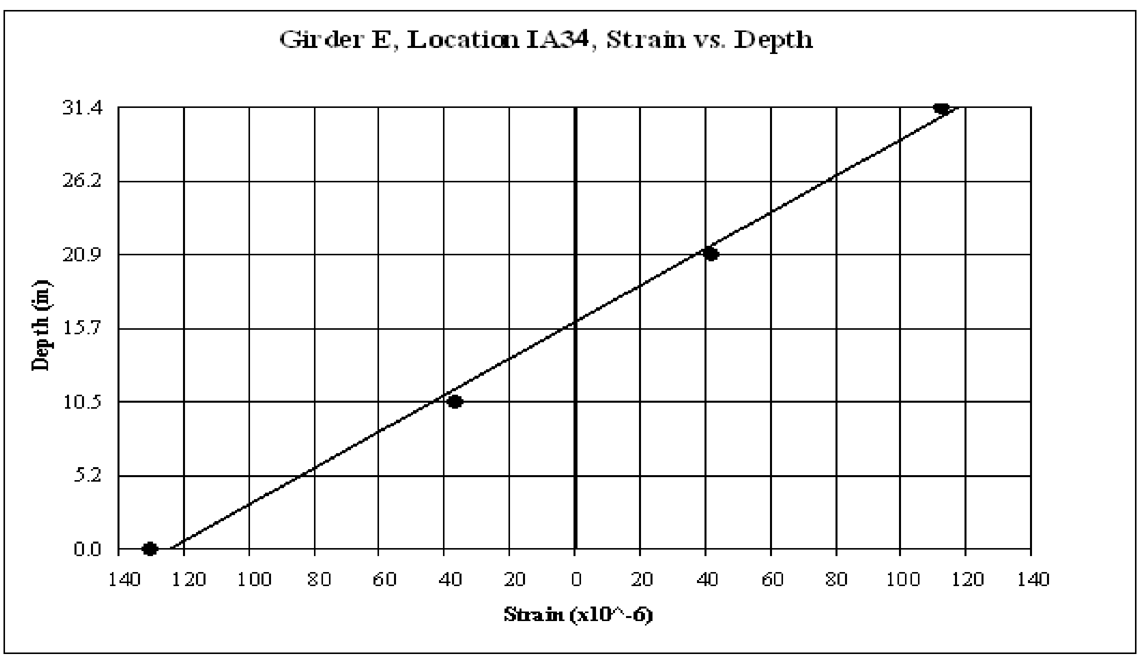

Figure 5: Girder E, Location IA34, Strain vs. Depth

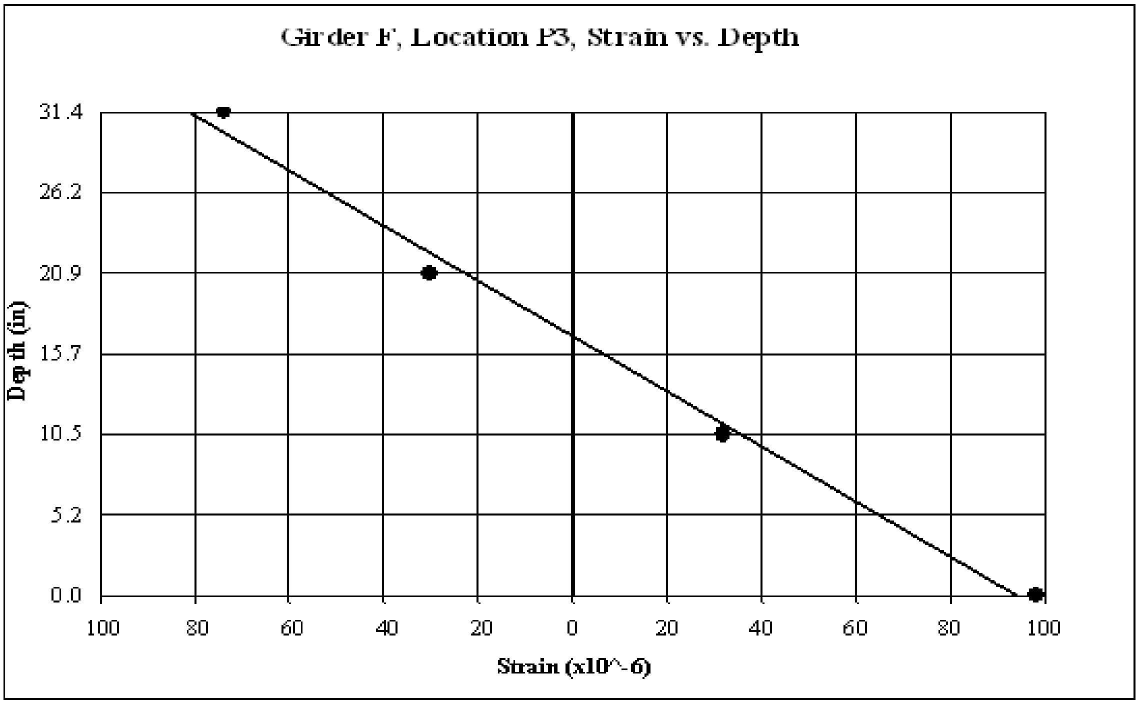

Figure 6: Girder F, Location P3, Strain vs. Depth

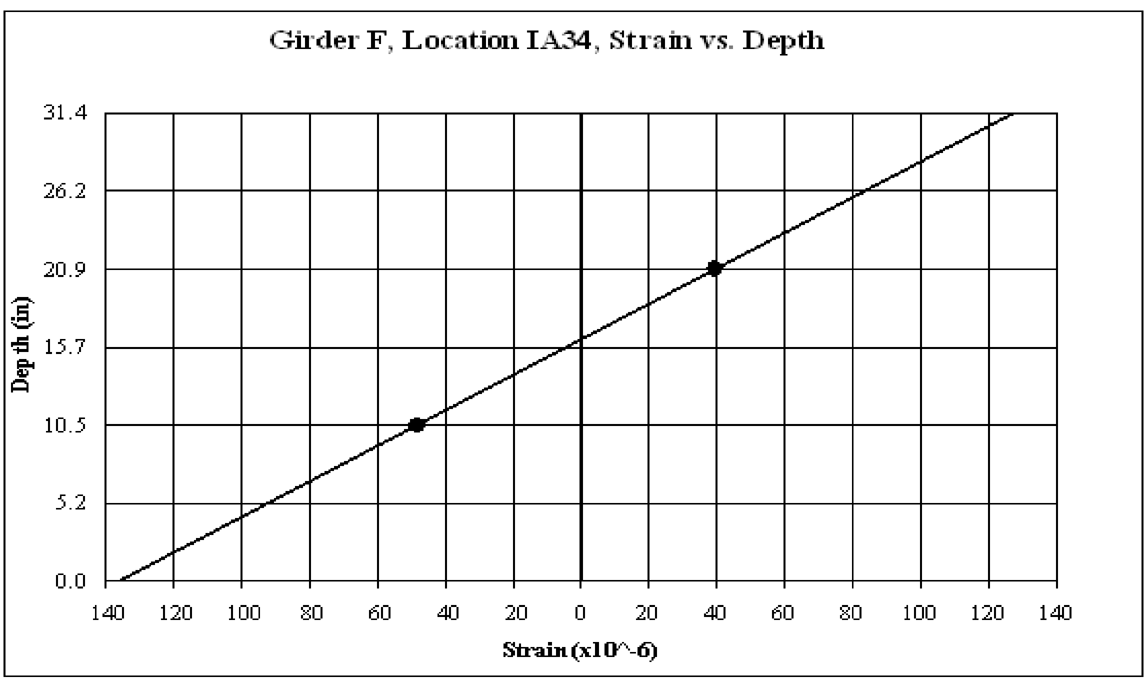

Figure 7: Girder F, Location IA34, Strain vs. Depth

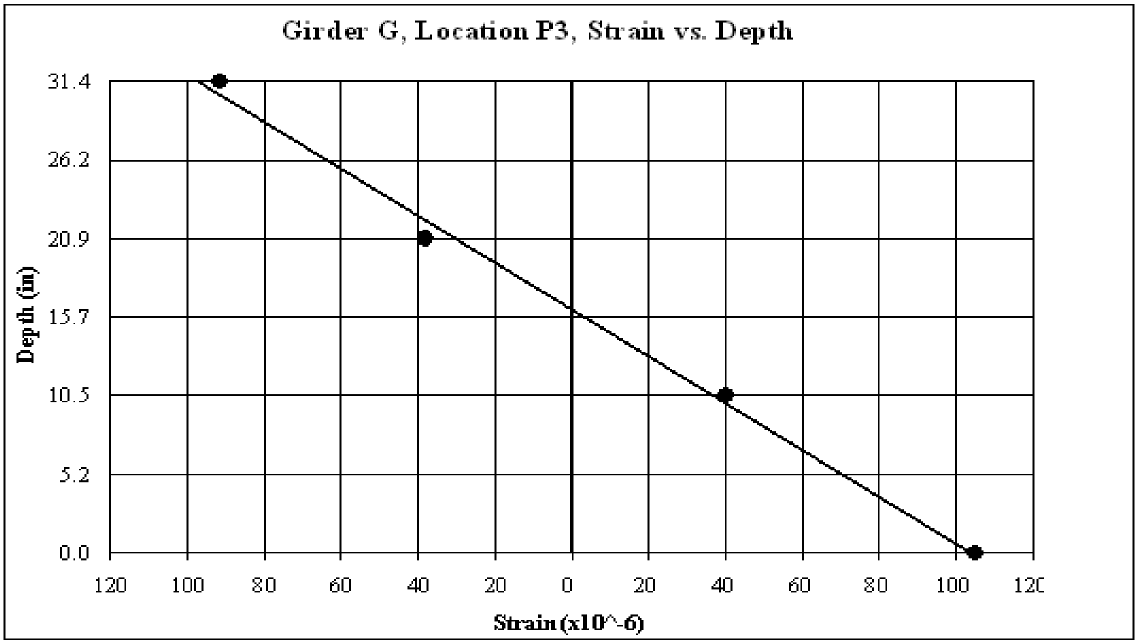

Figure 8: Girder G, Location P3, Strain vs. Depth

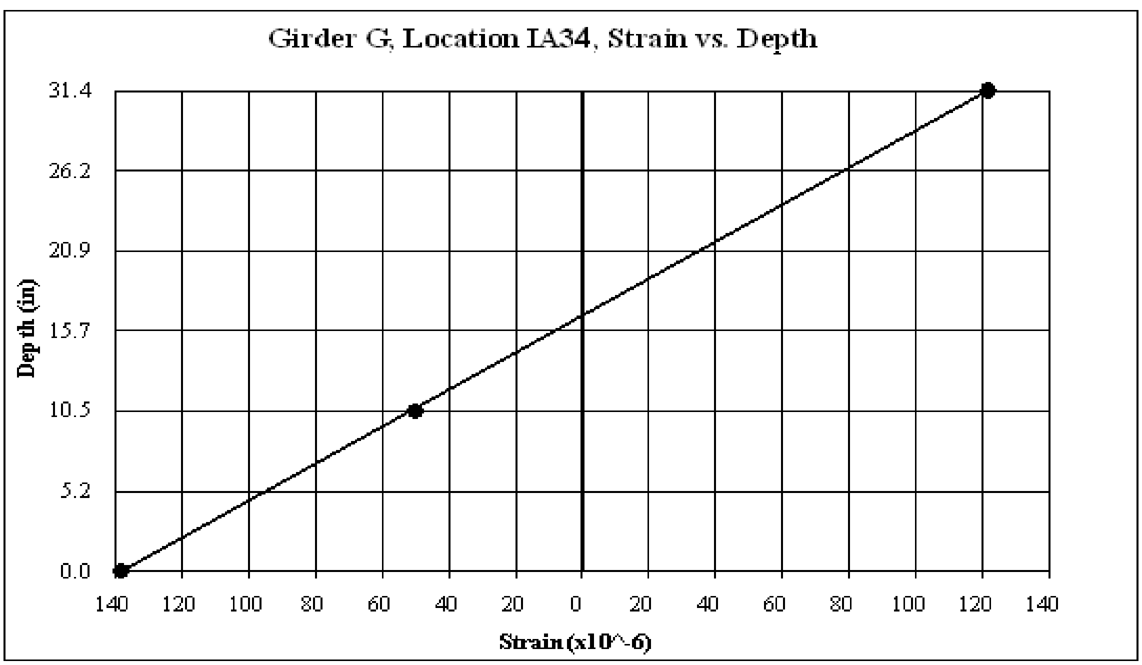

Figure 9: Girder G, Location IA34, Strain vs. Depth

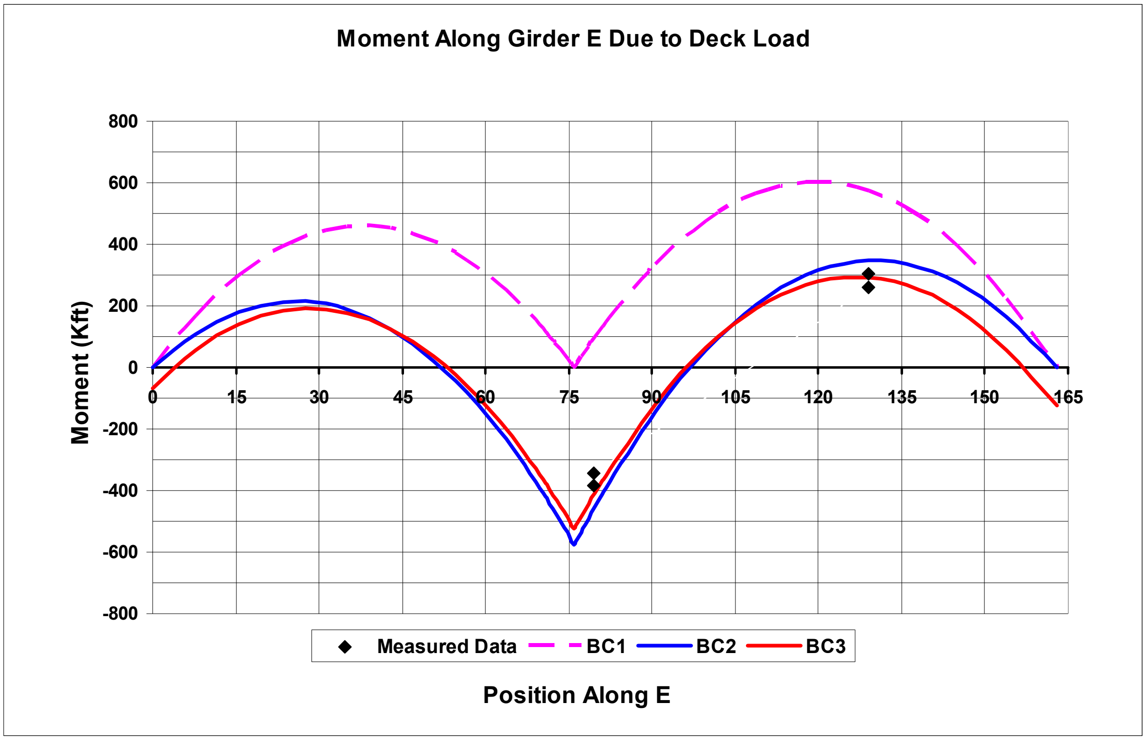

Figure 10: Moment Diagram (Girder E)

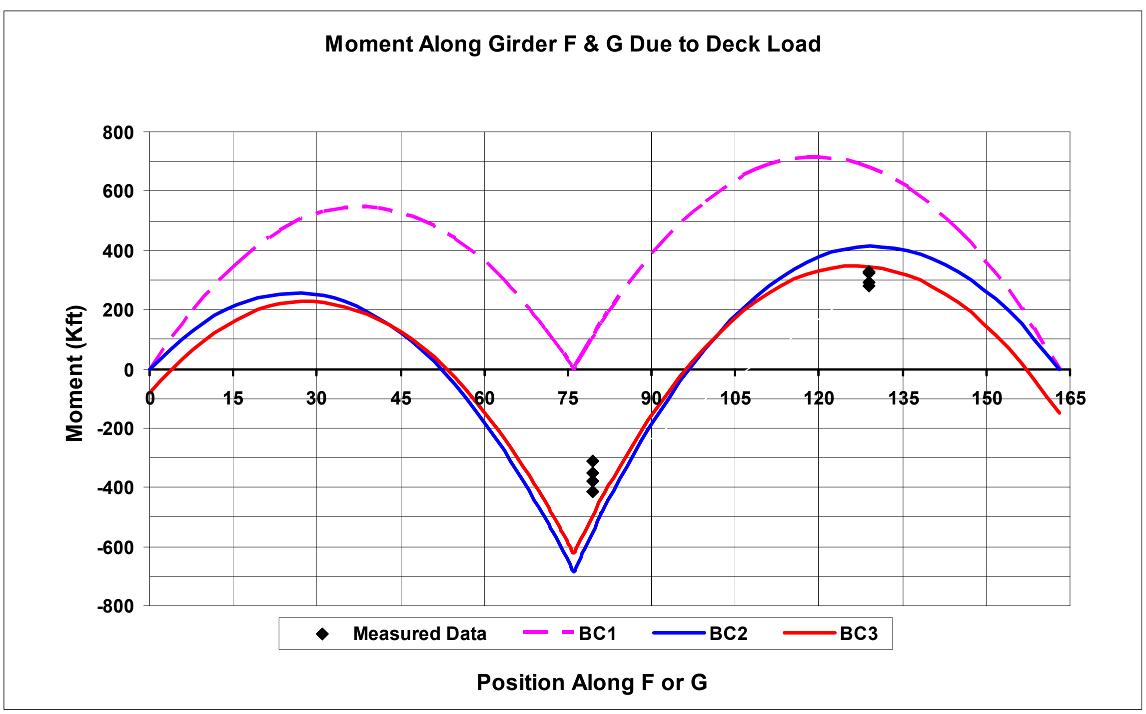

Figure 11: Moment Diagram (Girder F & G)

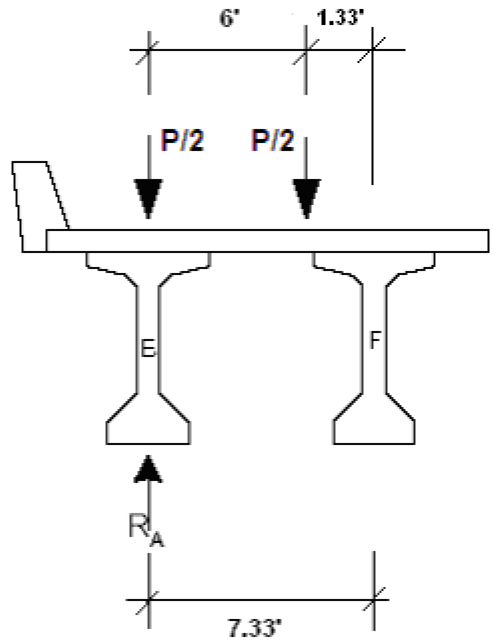

Figure 12: Truck Location on Exterior Girder

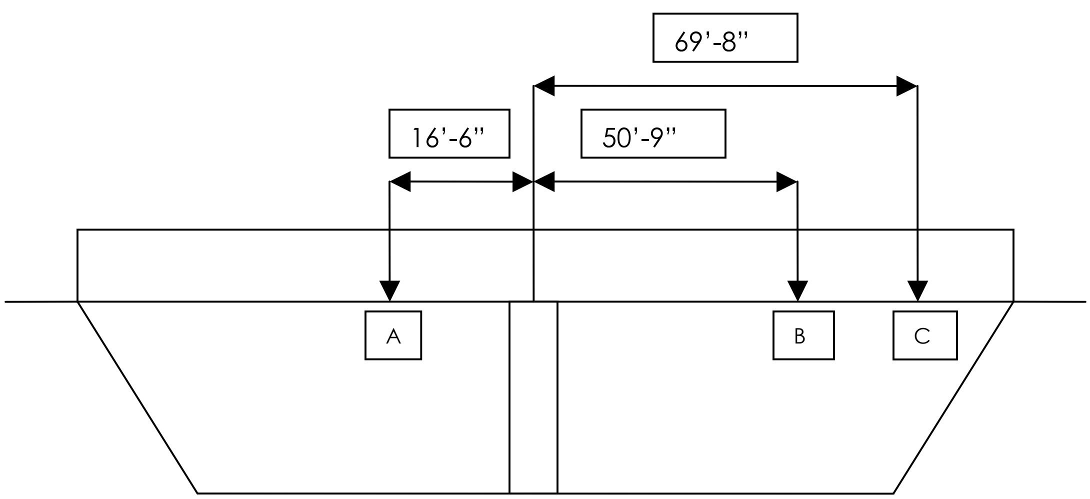

Figure 13: Longitudinal Truck Positions

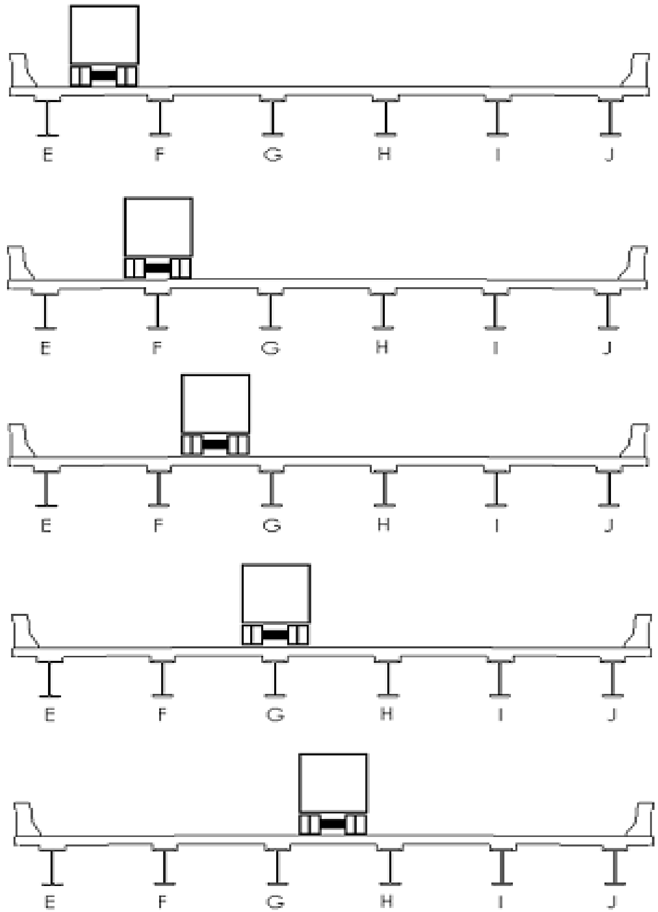

Figure 14: Lateral Truck Location

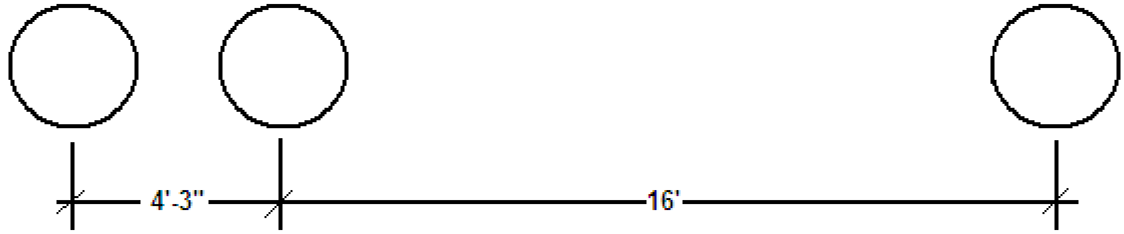

Figure 15: Truck Wheel Spacing

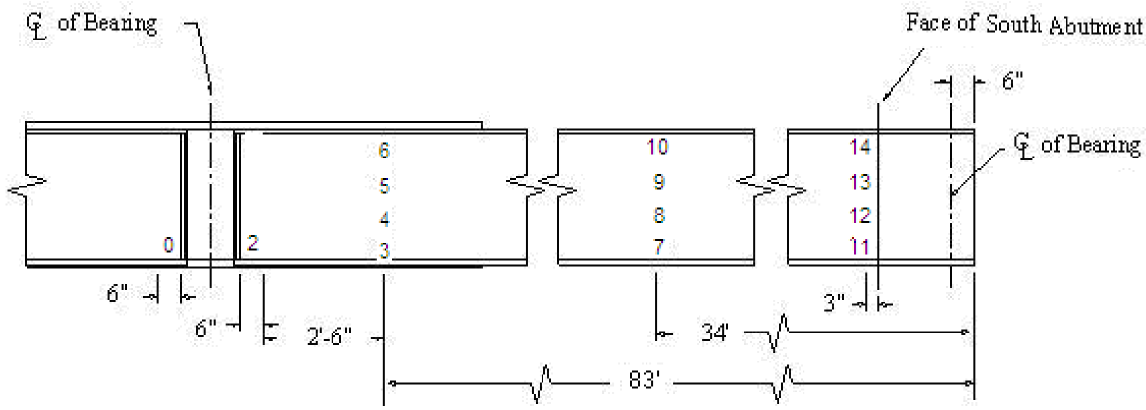

Figure 16: Longitudinal Gage Position on a Girders

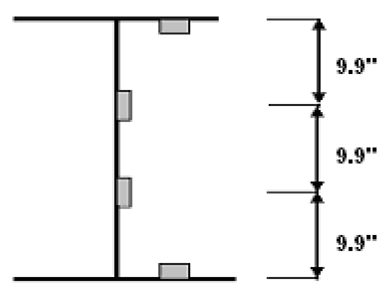

Figure 17: Section Showing Gage Position on Girder

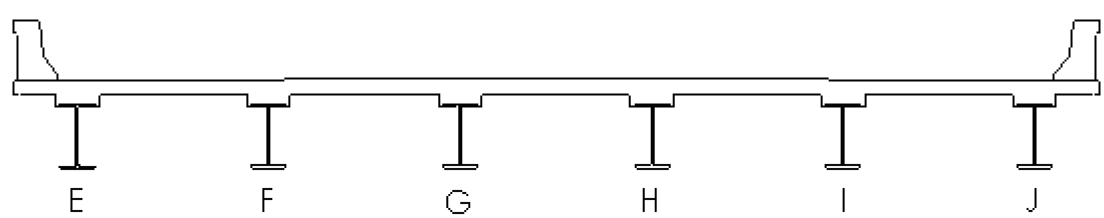

Figure 18: Steel Girders and Concrete Deck of Bridge

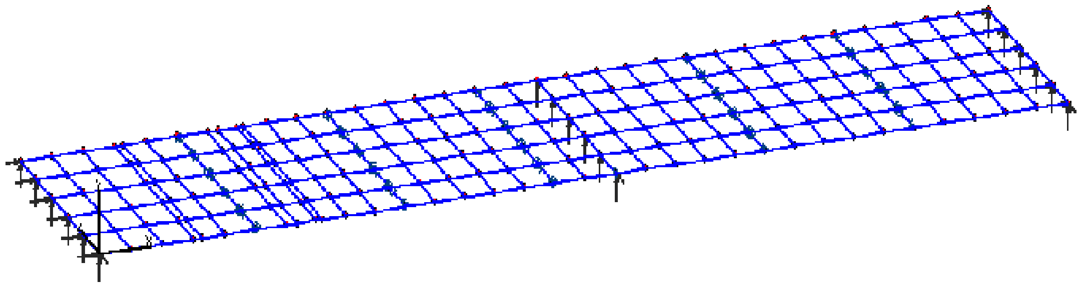

Figure 19: Mesh of the Superstructure

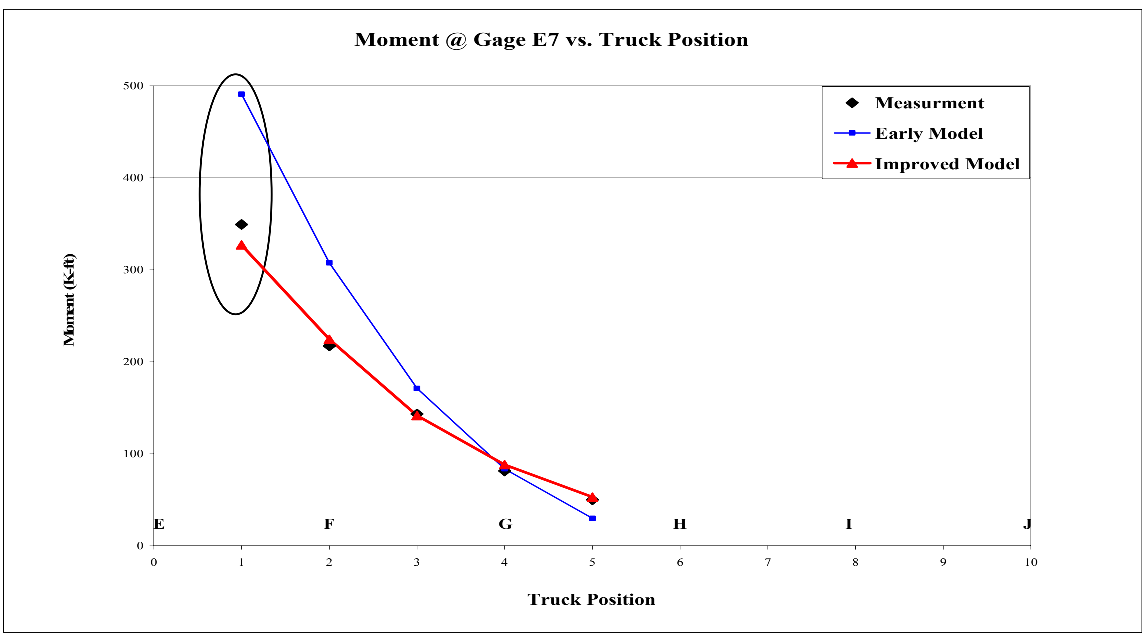

Figure 20: Comparison of Output from Early Model and Improved Model (1)

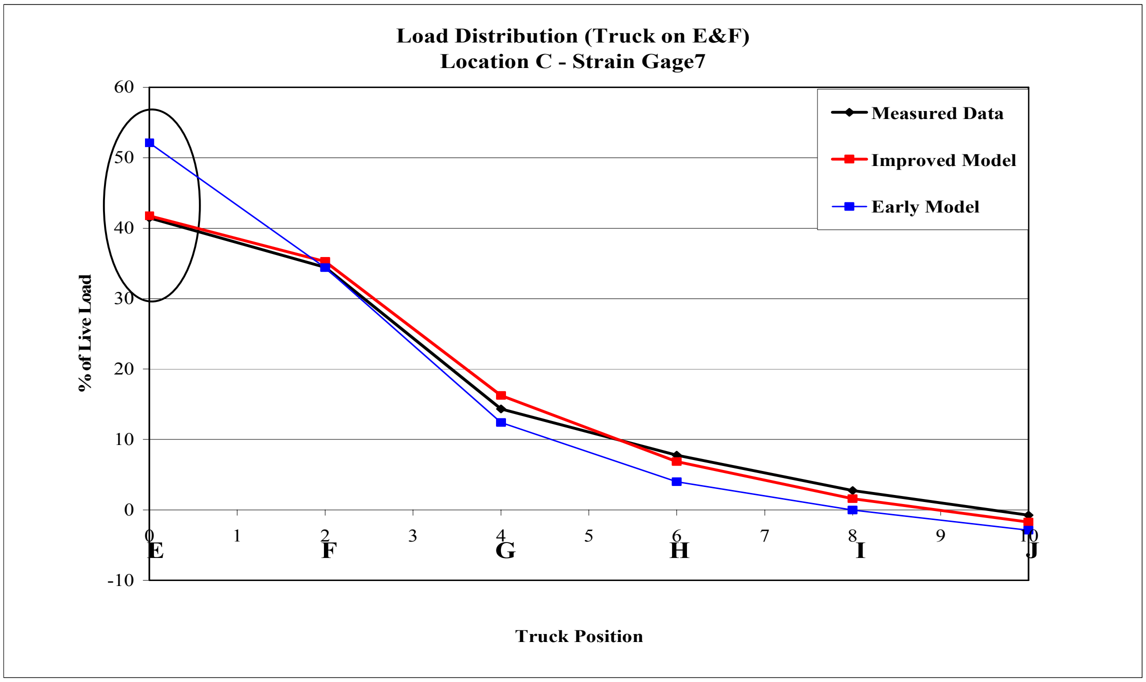

Figure 21: Comparison of Output from Early Model and Improved Model (2)

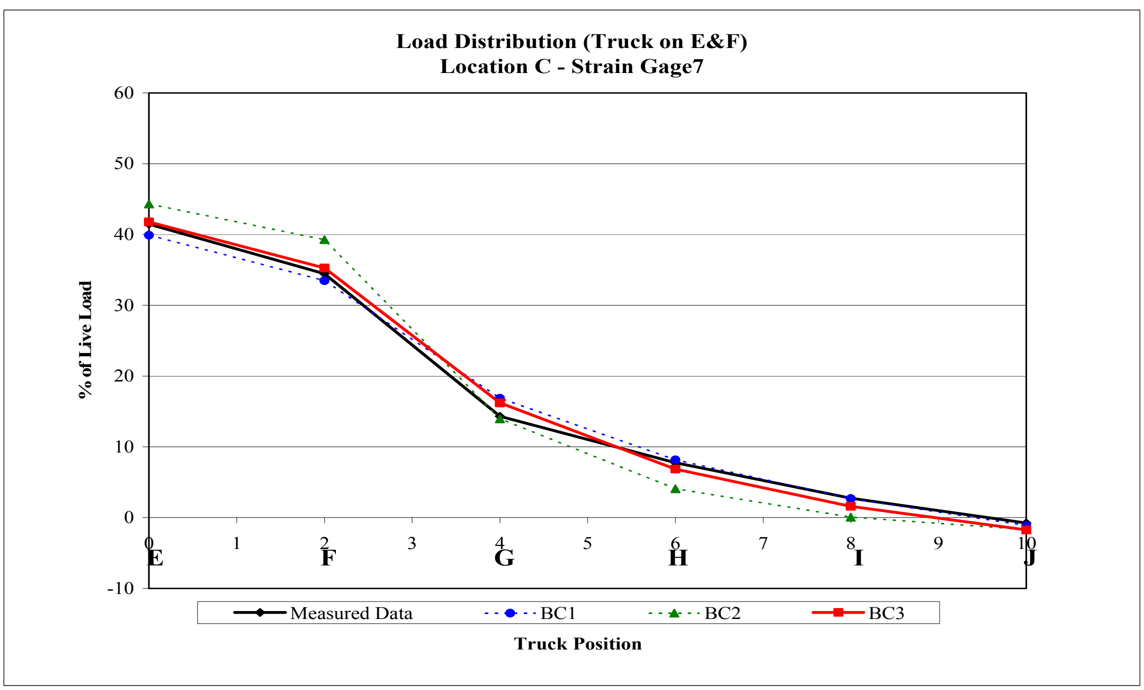

Figure 22: Lateral Distribution of the Moment (Strain Gage 7) in Girders with the Truck Load on Location C Girder E & F

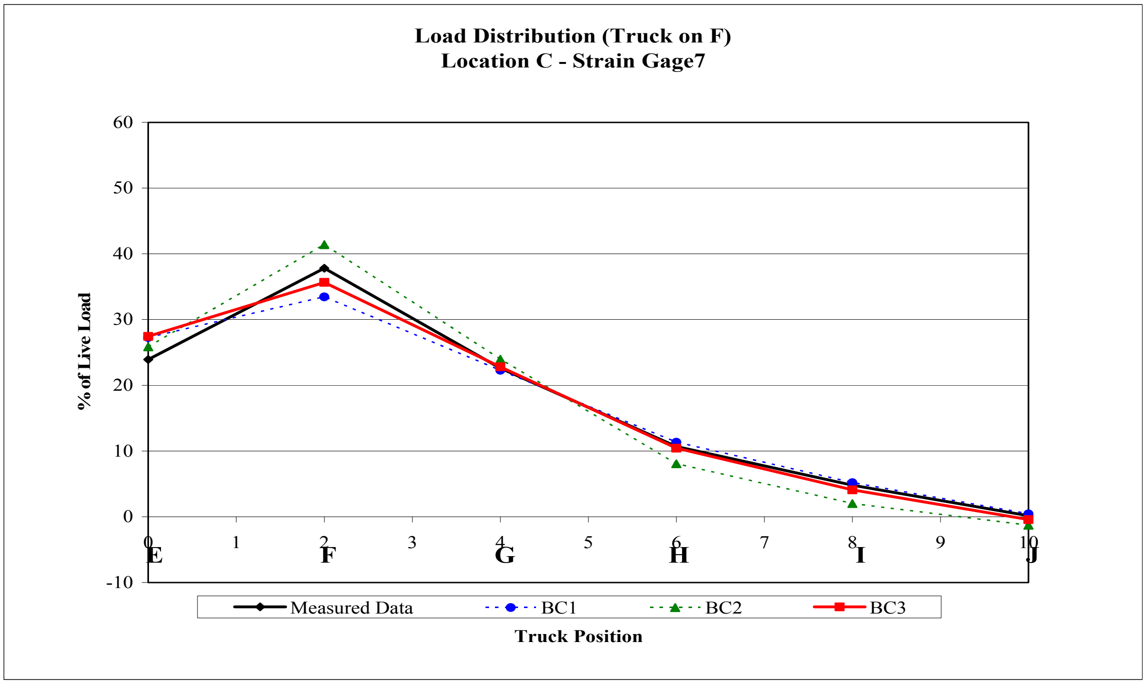

Figure 23: Lateral Distribution of the Moment (Strain Gage 7) in Girders with the Truck Load on Location C Girder F

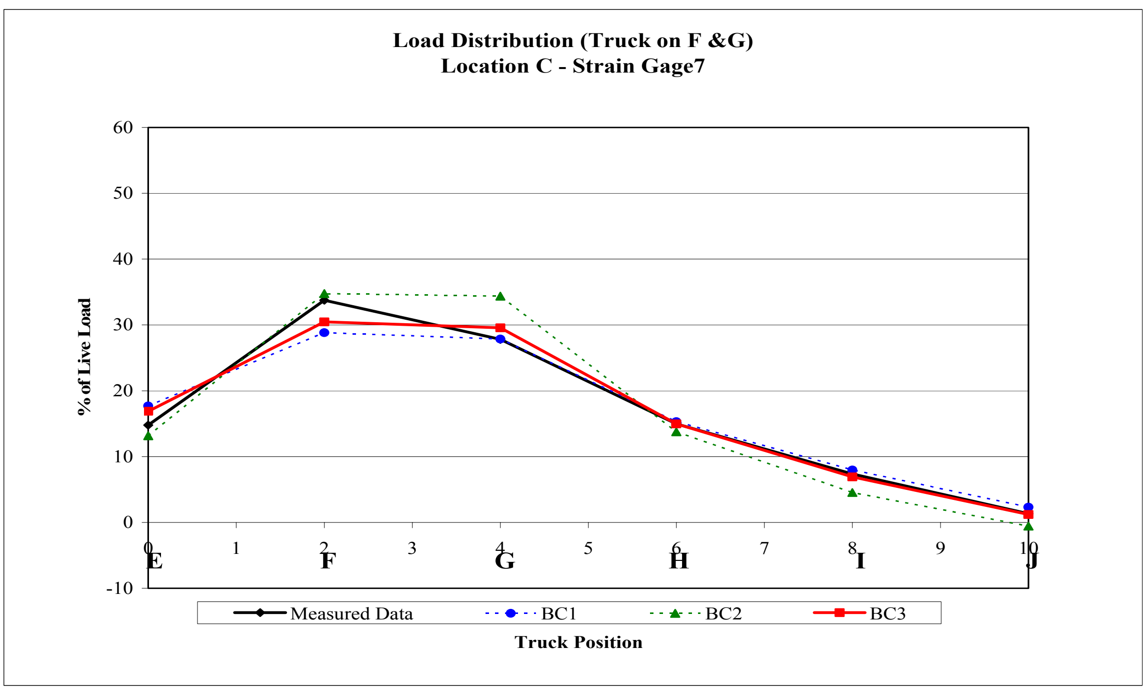

Figure 24: Lateral Distribution of the Moment (Strain Gage 7) in Girders with the Truck Load on Location C Girder F & G

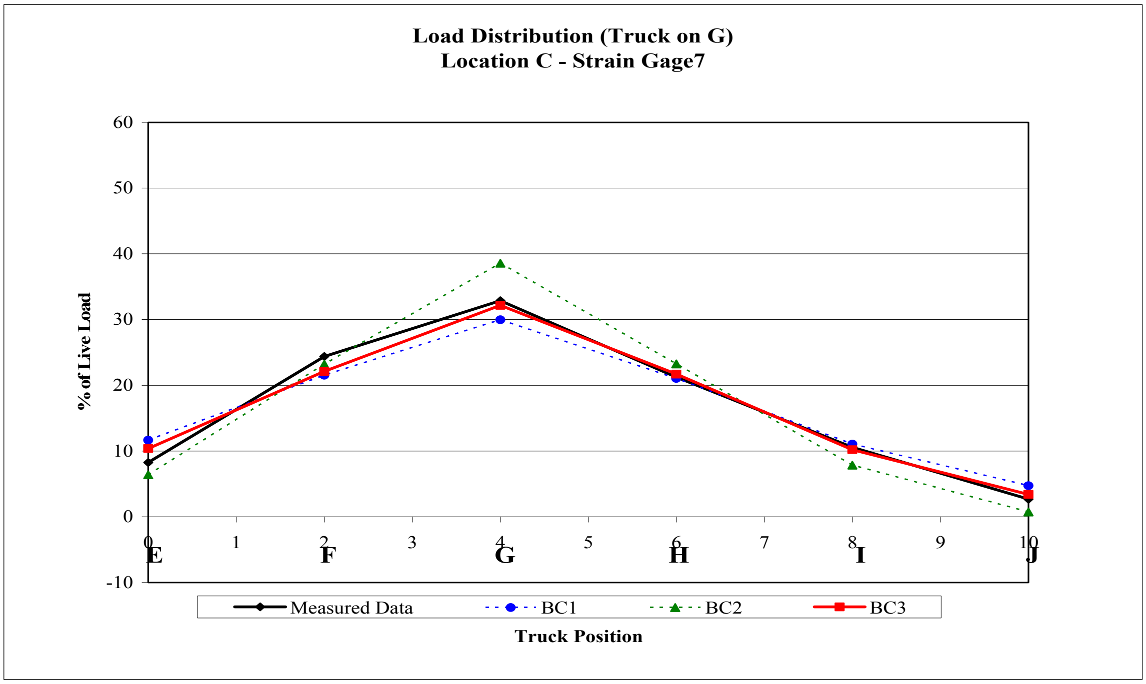

Figure 25: Lateral Distribution of the Moment (Strain Gage 7) in Girders with the Truck Load on Location C Girder G

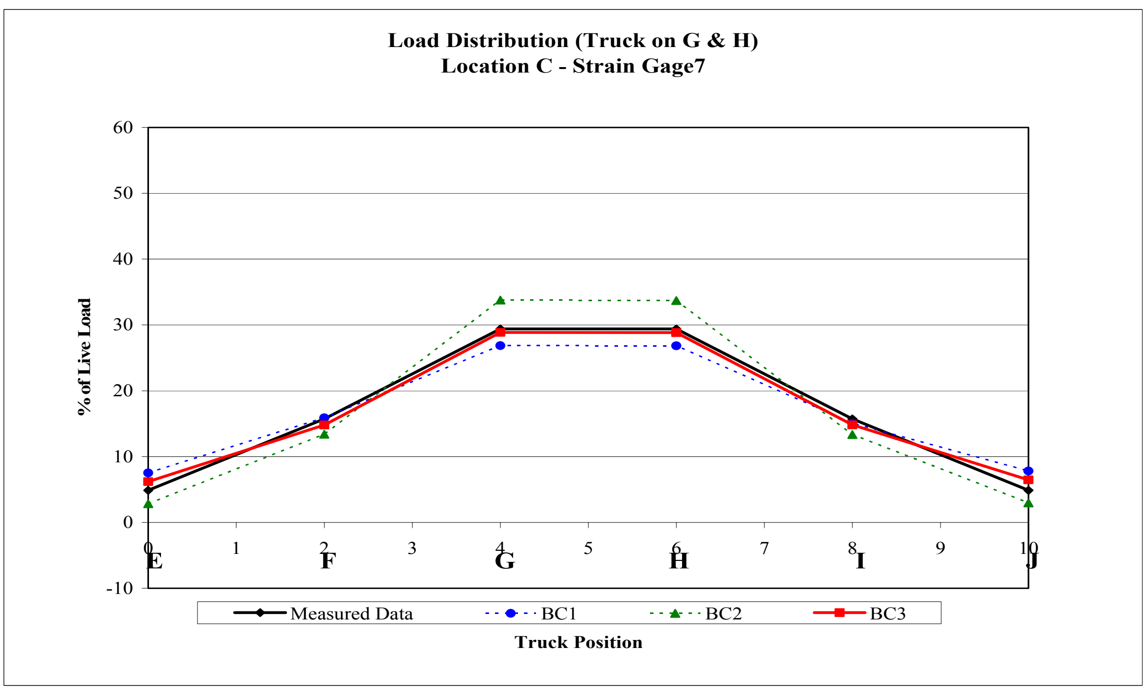

Figure 26: Lateral Distribution of the Moment (Strain Gage 7) in Girders with the Truck Load on Location C Girder G &H

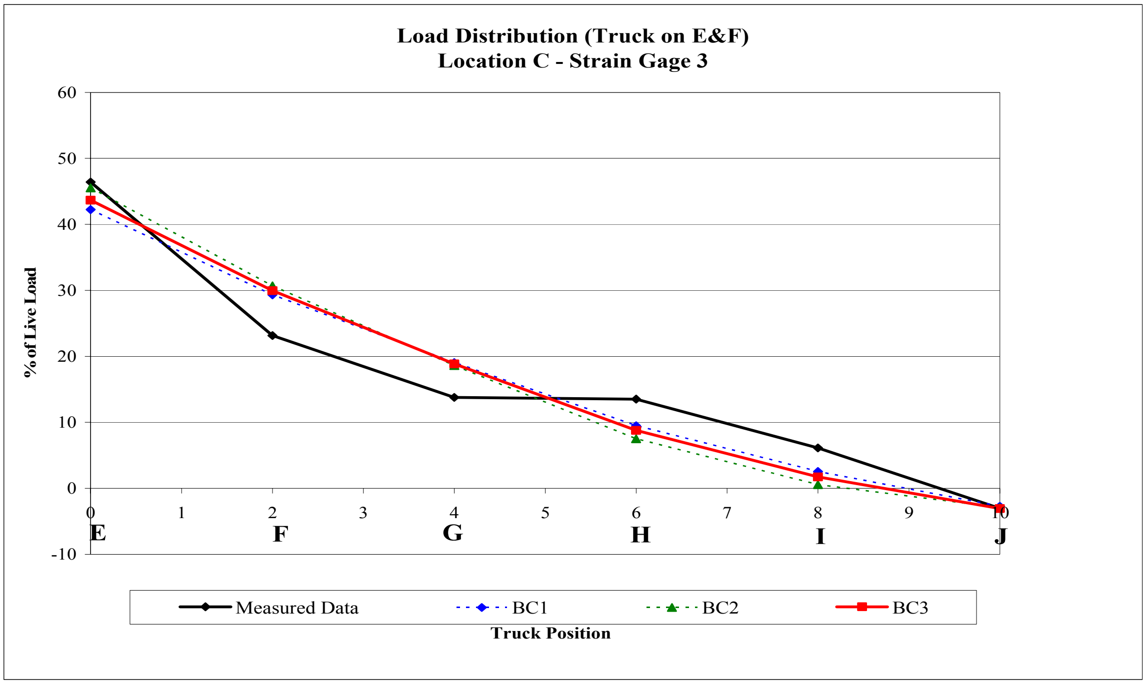

Figure 27: Lateral Distribution of the Moment (Strain Gage 3) in Girders with the Truck Load on Location C Girder E & F

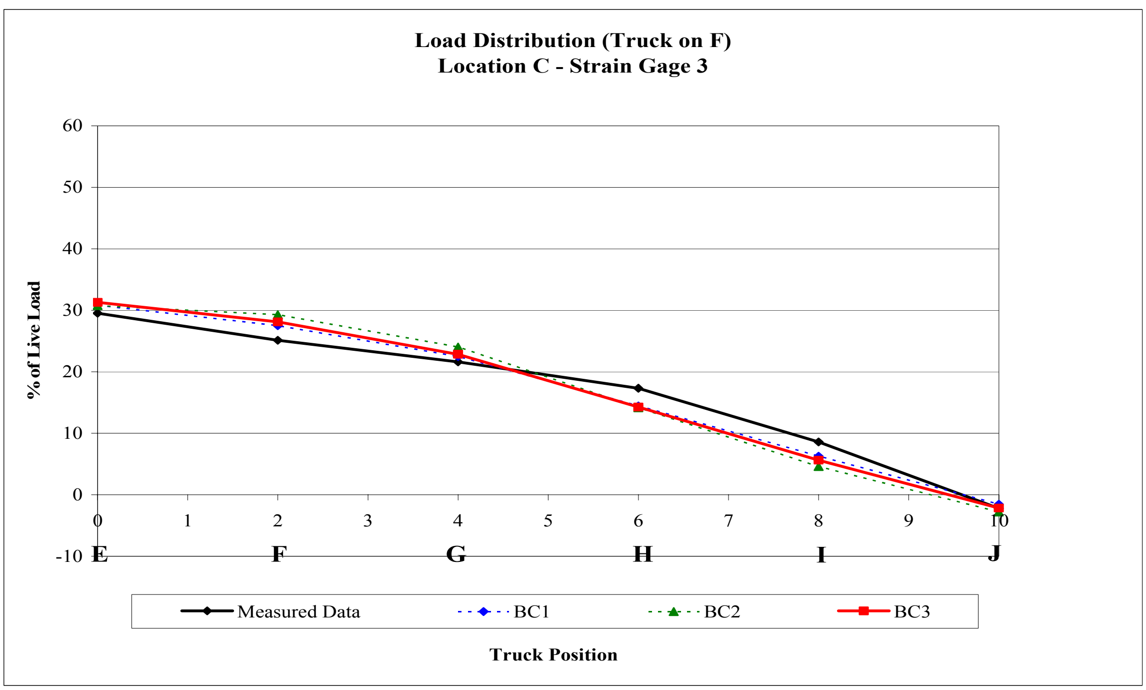

Figure 28: Lateral Distribution of the Moment (Strain Gage 3) in Girders with the Truck Load on Location C Girder F

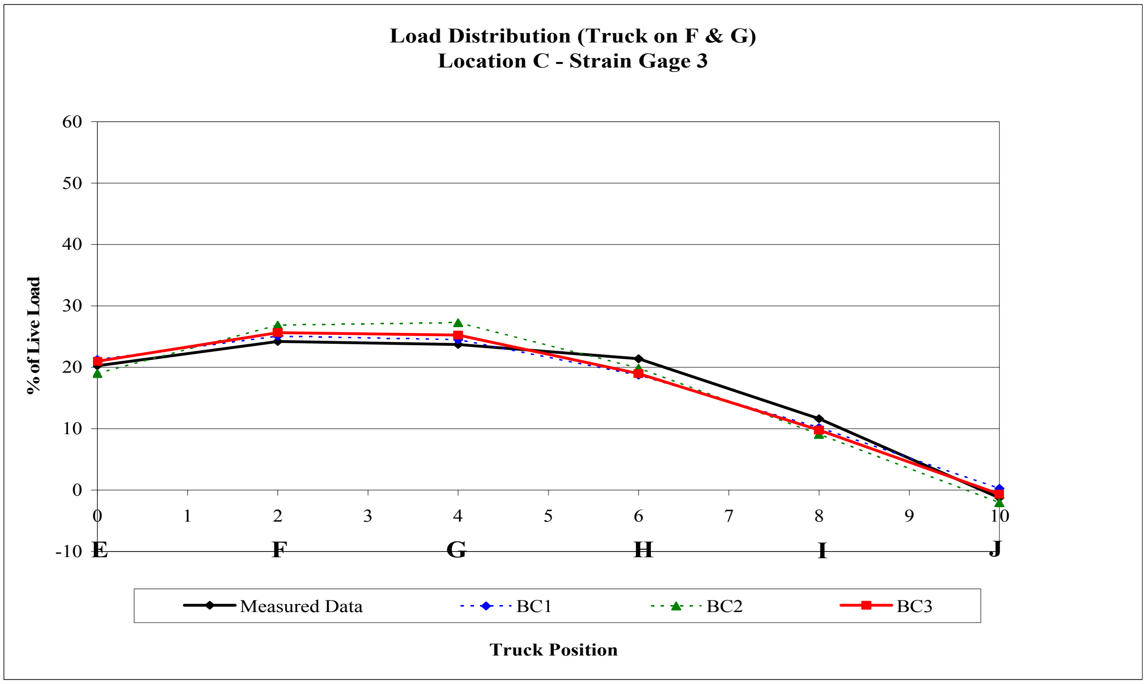

Figure 29: Lateral Distribution of the Moment (Strain Gage 3) in Girders with the Truck Load on Location C Girder F & G

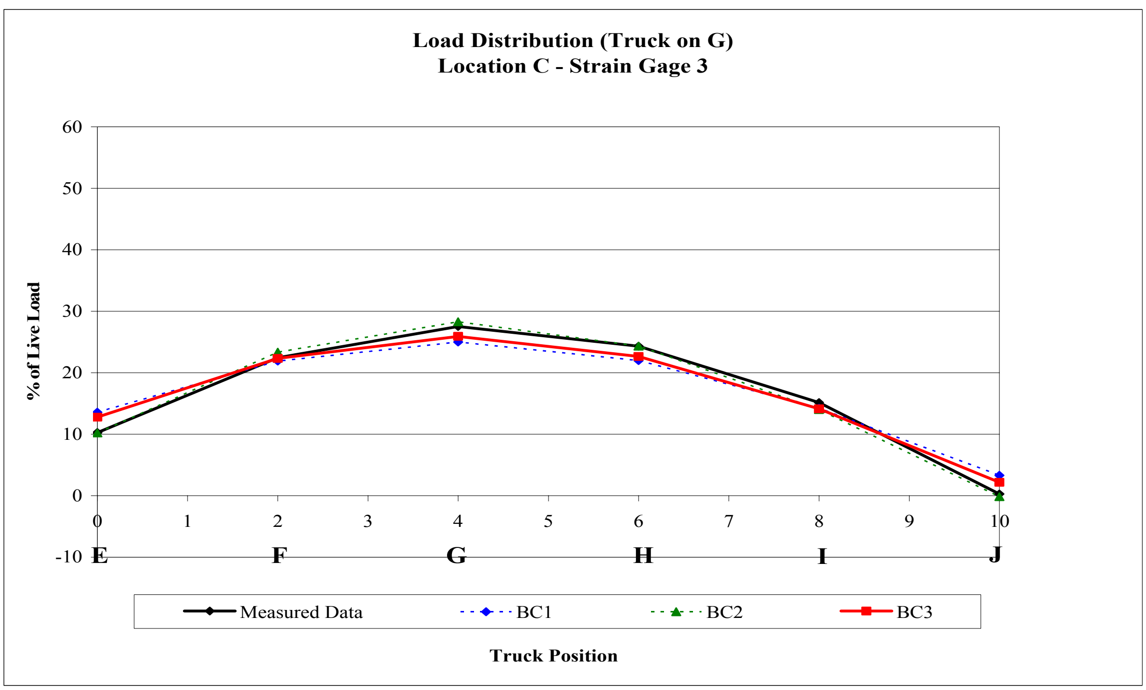

Figure 30: Lateral Distribution of the Moment (Strain Gage 3) in Girders with the Truck Load on Location C Girder G

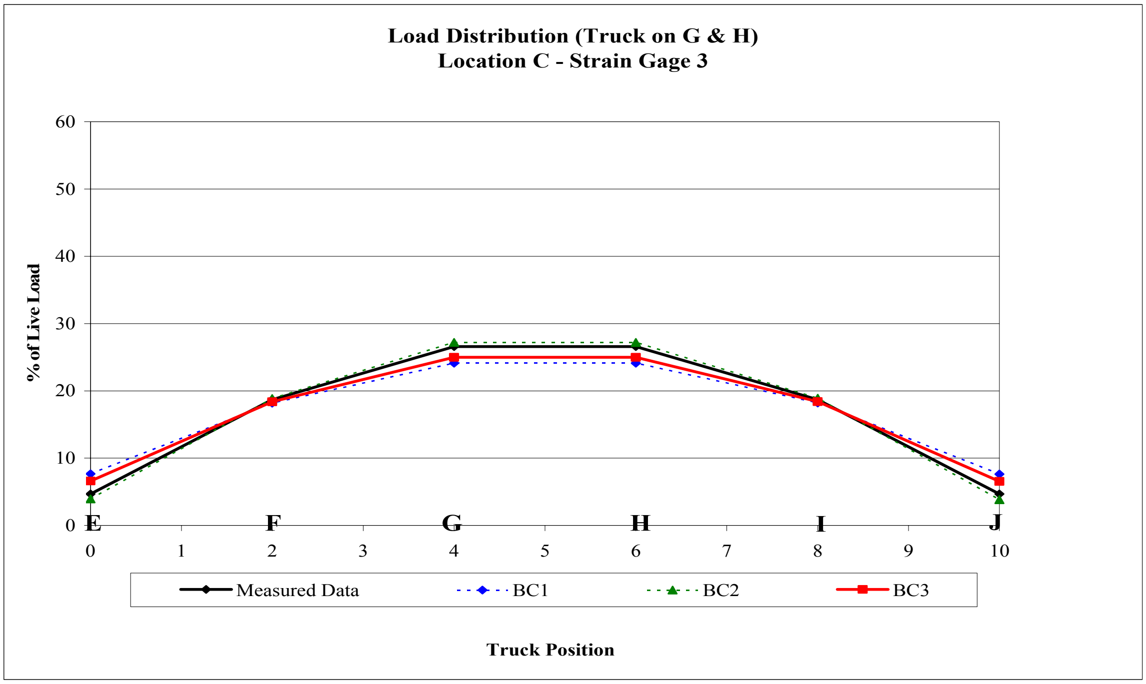

Figure 31: Lateral Distribution of the Moment (Strain Gage 3) in Girders with the Truck Load on Location C Girder G & H

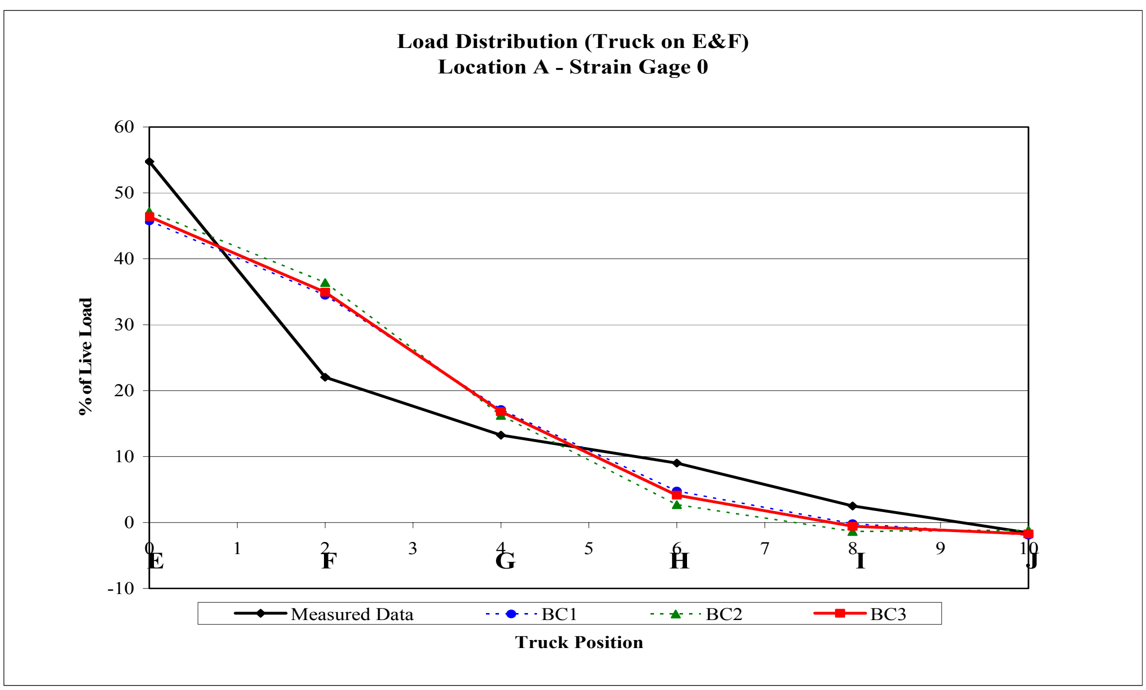

Figure 32: Lateral Distribution of the Moment (Strain Gage 0) in Girders with the Truck Load on Location A Girder E &F

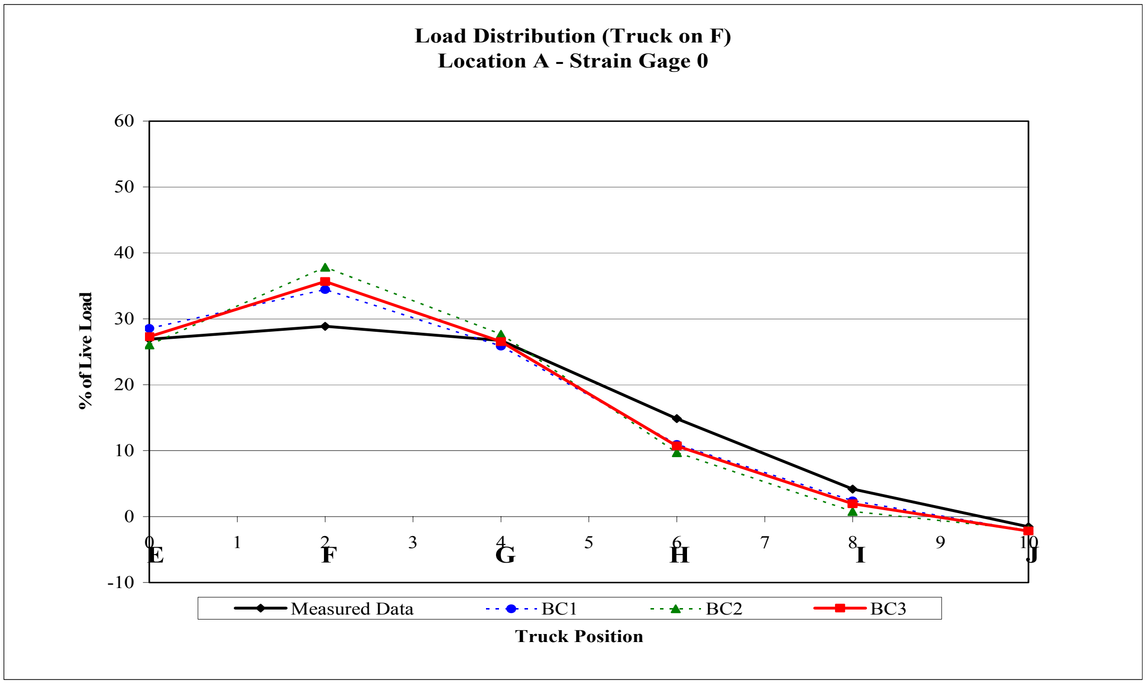

Figure 33: Lateral Distribution of the Moment (Strain Gage 0) in Girders with the Truck Load on Location A Girder F

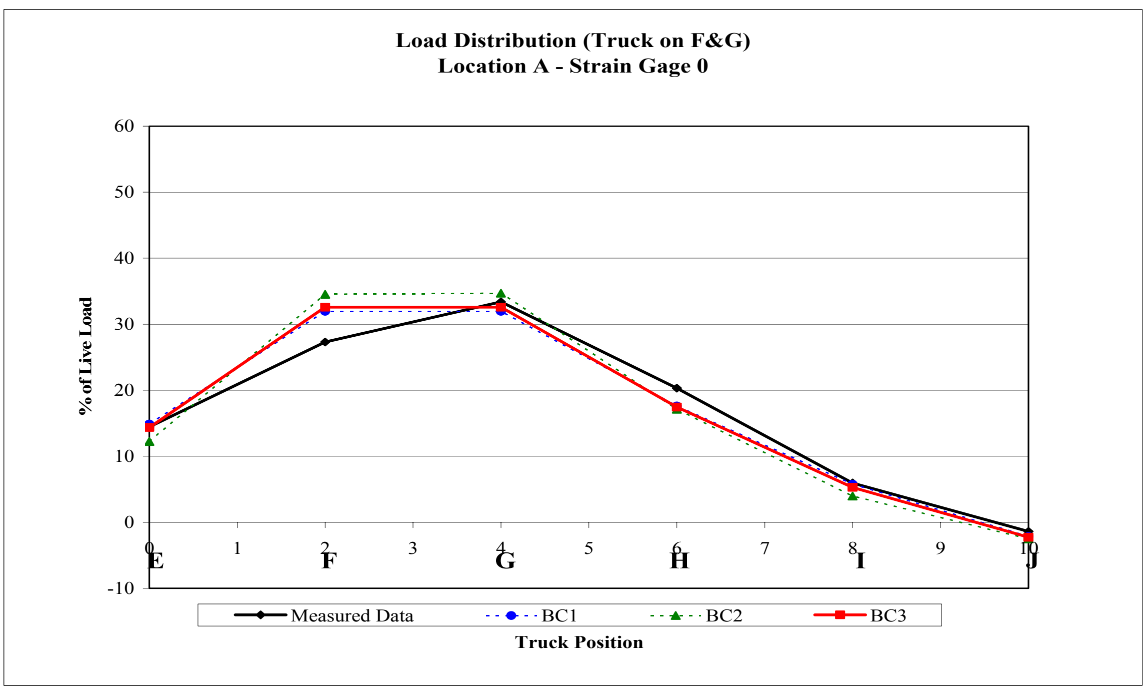

Figure 34: Lateral Distribution of the Moment (Strain Gage 0) in Girders with the Truck Load on Location A Girder F & G

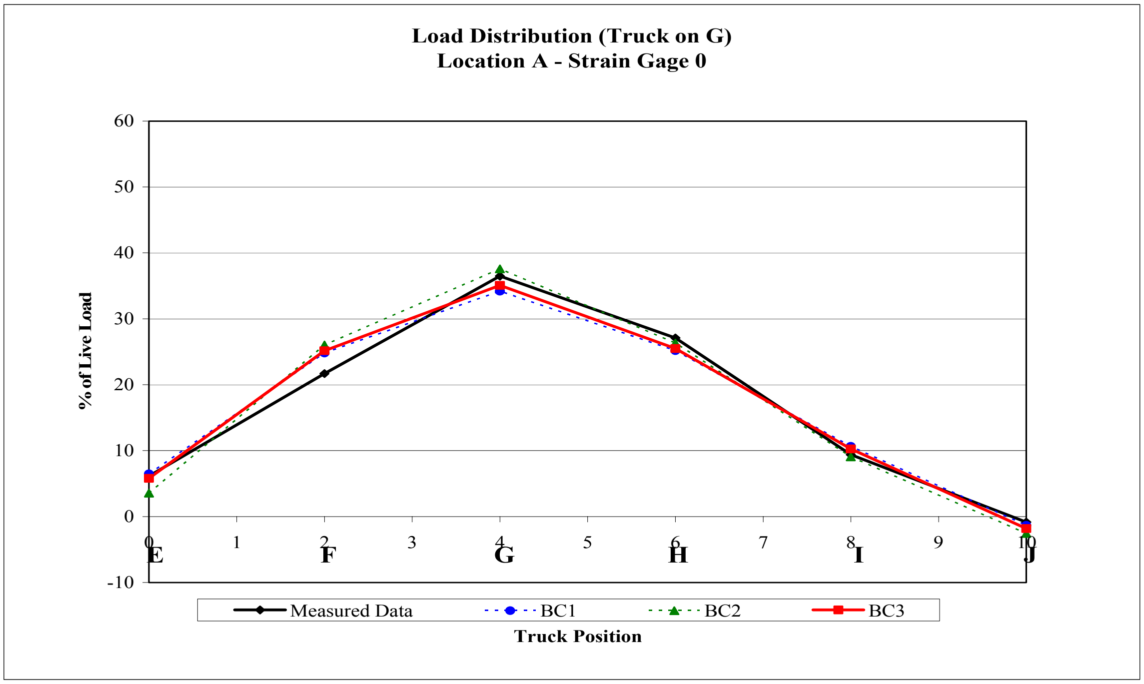

Figure 35: Lateral Distribution of the Moment (Strain Gage 0) in Girders with the Truck Load on Location A Girder G

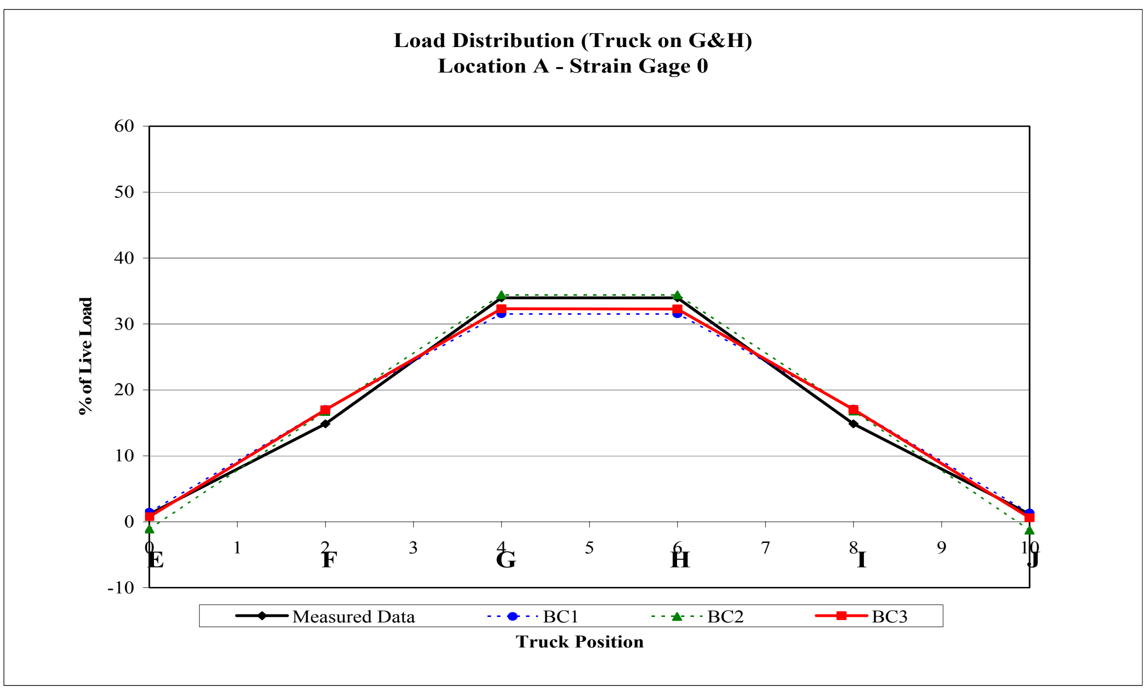

Figure 36: Lateral Distribution of the Moment (Strain Gage 0) in Girders with the Truck Load on Location A Girder G & H

Vita

Naiyu Wang was born on April 16, 1979 in LinZe, Gansu Province, China. She attend the University of Electronic Science and Technology of China (UESTC) in Sichuan Province and received a Bachelors of Science in the Fall of 2000. Ms. Wang started her Master's in the Fall of 2003 at University of Tennessee and received a Masters of Science in Civil Engineering in the Summer of 2005.